Discovery of positive and purifying selection in metagenomic time series of hypermutator microbial populations

Rohan Maddamsetti[1, †*] and Nkrumah A. Grant[2,3,4,†*]

[1]Department of Biomedical Engineering, Duke University, Durham, NC
[2]BEACON Center for the Study of Evolution in Action, Michigan State University, East Lansing, MI
[3]Department of Microbiology and Molecular Genetics, Michigan State University, East Lansing, MI
[4]Department of Biological Sciences, University of Idaho, Moscow, ID
[†]Joint first author
[*]Correspondence to: rohan.maddamsetti@gmail.com, nkrumah.grant88@gmail.com

Short title: positive and purifying selection in hypermutators

ABSTRACT

A general method to infer both positive and purifying selection during the real-time evolution of hypermutator pathogens would be broadly useful. To this end, we introduce a simple test to infer mode of selection (STIMS) from metagenomic time series of evolving microbial populations. We test STIMS on metagenomic data generated by simulations of bacterial evolution, and on metagenomic data spanning 62,750 generations of Lenski's long-term evolution experiment with *Escherichia coli* (LTEE). In both cases, STIMS recovers signals of positive and purifying selection on gold standard sets of genes. Using STIMS, we find strong evidence of ongoing positive selection on key regulators of the *E. coli* gene regulatory network, even in some hypermutator populations. STIMS also detects positive selection on regulatory genes in hypermutator populations of *Pseudomonas aeruginosa* that adapted to subinhibitory concentrations of colistin – an antibiotic of last resort – for just twenty-six days of laboratory evolution. Our results show that the fine-tuning of gene regulatory networks is a general mechanism for rapid and ongoing adaptation. The simplicity of STIMS, together with its intuitive visual interpretation, make it a useful test for positive and purifying selection in metagenomic data sets that track the evolution of hypermutator populations in real-time.

Keywords: positive selection, purifying selection, experimental evolution, metagenomics, gene regulatory network, hypermutators

INTRODUCTION

Organisms often evolve defects in DNA repair and recombination pathways that cause very high mutation rates. Hypermutability is readily observed in cancer [1-3] and in opportunistic pathogens attacking immunocompromised individuals [4]. Hypermutability is also associated with the evolution of antibiotic resistance, including multi-drug-resistant tuberculosis [5]. Hypermutability can increase the rate of beneficial mutations, but it can also obscure the genomic basis of adaptation [6], because vast numbers of nearly-neutral mutations hitchhike to high frequencies with the beneficial mutations that drive the selection dynamics. In this regime, called "emergent neutrality" [7], it is challenging to identify selection on particular genes, unless those genes are under very strong selection [8, 9]. As such, there is a need for methods that can resolve positive and purifying selection in hypermutator populations, due to their importance in basic research, genetic engineering, and medicine. To address this research gap, we present a simple test to infer mode of selection (STIMS) from metagenomic time series of large asexual hypermutator populations, and use this method to study positive and purifying selection in bacterial populations that evolved hypermutability during long-term experimental evolution.

We developed STIMS in the context of Lenski's long-term evolution experiment with *Escherichia coli* (LTEE) [10, 11]. The LTEE has become an important test bed for many fundamental questions in evolutionary biology, due to its simplicity (daily serial transfer of twelve populations) and comprehensive record of frozen bacterial samples. Previous studies have used the LTEE as a model system to study the tempo and mode of both genomic [12-16] and phenotypic evolution [10, 17-22]. Many of those previous studies focused on the evolutionary dynamics underlying adaptive evolution. The evolution of hypermutability in six of the LTEE populations has obscured the genomic signatures of adaptation [6, 12, 15, 16, 23], again due to emergent neutrality. STIMS gains statistical power to infer selection despite emergent neutrality, by aggregating mutations within a focal set of genes, counting their occurrence, then comparing the counts to a background distribution of the number of mutations per gene set.

This work expands on previous observations suggesting the action of purifying selection on hypermutator populations of the LTEE [21]. In that work, we found that aerobic-specific genes were depleted in mutations compared to randomized sets of genes in three hypermutator populations: Ara−2, Ara+3, and Ara+6. That finding suggests that aerobic-specific genes may

have transitioned from positive selection to purifying selection in those LTEE populations [21]. Our work also complements recent findings of purifying selection affecting protein evolution [24] and protein-protein-interaction network evolution in the LTEE [25].

Here, we demonstrate that STIMS recovers signals of positive and purifying selection in evolutionary simulations of haploid populations under a Wright-Fisher model, and show that STIMS recovers signals of positive and purifying selection on gold-standard sets of genes with *a priori* evidence of those selection pressures in the LTEE. We then use STIMS to examine the *tempo* of molecular evolution in modules of co-regulated genes [26-28], and to generate testable hypotheses about the *mode* (i.e. purifying or positive selection) of evolution on those gene modules in the LTEE. Finally, we use STIMS to test for positive selection on regulatory genes in a 26-day evolution experiment involving adaptation of hypermutator *Pseudomonas aeruginosa* to subinhibitory concentrations of colistin, an antibiotic of last resort. These results indicate that STIMS is a useful and general test for selection, even over relatively short timescales of molecular evolution.

RESULTS

Simulations demonstrate the conditions in which STIMS is an effective test for positive and purifying selection

The key premise of STIMS is that the tempo of molecular evolution differs across different sets of genes, due to variation in the underlying selection pressures affecting those sets of genes. As input, STIMS requires a list of mutations that have been observed in metagenomic sequencing of a haploid population, sampled over time (Figure 1). STIMS then calculates a simple summary statistic of the evolutionary dynamics: the number of observed mutations in a query gene set, normalized by total gene length. A *p*-value is then calculated using the non-parametric bootstrap, which is simply a count of the times that a random gene set accumulates more mutations than the query gene set (Figure 2). The same logic applies when measuring whether a gene set is depleted of mutations: in this case, STIMS counts the number of times that a random selection of genes accumulates fewer mutations than the query gene set. Importantly, the bootstrapped background distribution does *not*, in general, correspond to a neutral null model

101 of evolution: genome-wide positive and purifying selection may affect the background
102 distribution. Accordingly, STIMS is interpreted in relation to the overall tempo at which
103 mutations are observed across the genome in a given population, which is driven by population-
104 genetic parameters such as mutation rate, population size, and the genomic distribution of
105 mutation fitness effects (DFE).

106 For this reason, we evolved haploid populations *in silico* using a Wright-Fisher model to
107 examine the conditions under which STIMS can detect positive and purifying selection in
108 idealized populations, in which the strength of selection on various regions of the genome is
109 known *a priori*. We ran 10 replicate simulations of nonmutator haploid populations and 10
110 replicate simulations of hypermutator haploid populations, using large population sizes, mutation
111 rates parameterized from LTEE measurements, and an idealized genome and DFE based on *E.*
112 *coli* (Materials and Methods). The results of these simulations, and our analysis of these
113 simulations using STIMS, are shown in Figure 3 for the nonmutator case and in Figure 4 for the
114 hypermutator case.

115 The dynamics of adaptation in our simulations are strikingly similar to the dynamics
116 observed in the LTEE: both the nonmutator populations (Figure 3A) and the hypermutator
117 populations (Figure 4A) show periodic selective sweeps, cohorts of mutations rising to fixation
118 simultaneously, and clonal interference. These patterns are characteristic of the evolution of large
119 asexual populations in which the supply of beneficial mutations does not limit adaptation [14, 16,
120 29]. Thus, our *in silico* simulations are representative of the biology we aim to describe.

121 We designed the genomes of our simulated haploid populations such that we knew *a*
122 *priori* the mode of selection acting on particular genomic regions. Therefore, we used our
123 simulated data to evaluate how well STIMS could detect selection given that it exists
124 (sensitivity), and avoid false positives (specificity). Our simulations demonstrate that STIMS has
125 both high sensitivity and specificity in detecting positive selection in both nonmutator and
126 hypermutator populations (Figures 3B and 4B). Most mutations observed in the nonmutator
127 populations are beneficial. So, the background distribution for the nonmutator populations
128 reflects positive selection on beneficial driver mutations and the dynamics of passenger
129 mutations hitchhiking with those driver mutations. In the nonmutator populations, not enough
130 mutations are observed across the genome to see which genes are depleted of passenger
131 mutations. Consequently, STIMS cannot detect purifying selection in this context. Nevertheless,

132 STIMS is highly specific. It does not call any false positives in our tests for positive and
133 purifying selection in the nonmutator populations (Figure 3C). Representative visualizations of
134 STIMS when run on nonmutator populations are shown for genes evolving under positive
135 selection in Figure 3D, for genes evolving completely neutrally in Figure 3E, and for genes
136 evolving under purifying selection in Figure 3F. These visualizations show that for nonmutator
137 populations, gene modules with trajectories below the background distribution could be evolving
138 under purifying selection, or could be evolving completely neutrally due to relaxed selection.
139 This apparent difference from the background distribution is never statistically significant,
140 because most random gene sets have no mutations at all, and these empty sets are not plotted.
141 Gene modules with trajectories above the background distribution are evolving under strong
142 positive selection.

143 In contrast to the nonmutator populations, our simulations show that STIMS has high
144 sensitivity and specificity in detecting purifying selection in hypermutator populations (Figure
145 4C). In this case, mutation rates are high enough that passenger mutations arise densely across
146 the genome, allowing for the detection of genes that are depleted of observed passenger
147 mutations due to purifying selection. The sensitivity with which STIMS detects purifying
148 selection increases when 1) mutations can be reliably detected at lower frequencies; 2) the
149 number of genes in the gene set increases; 3) the interval between metagenomic sampling time is
150 smaller; and 4) the length of the time series increases (Figure 4C). All of these experimental
151 variables increase the resolution of the data and increase the ability of STIMS to detect purifying
152 selection in hypermutator populations. Representative visualizations of STIMS when run on
153 hypermutator populations are shown for genes evolving under positive selection in Figure 4D,
154 for genes evolving completely neutrally in Figure 4E, and for genes evolving under purifying
155 selection in Figure 4F.

156 These results show that STIMS is an effective test for selection, given sufficient data.
157 However, the realized DFE for microbial populations evolving in the laboratory or in nature may
158 deviate substantially from the idealized DFE in the simulations that we have presented. For this
159 reason, we validated STIMS on published metagenomic data tracking the allele frequency
160 dynamics in the LTEE, using three gold standard sets of genes with empirical evidence of
161 relaxed, purifying, and positive selection in the LTEE. These positive controls provide hard
162 evidence that STIMS is effective in practice.

Control 1: Resolving relaxed selection in the LTEE

As a first positive control, we examined 63 genes that have empirical evidence for neutral fitness effects in REL606 (A. Couce, personal communication). Figure 5 shows the results of applying STIMS on these genes, which we suppose are evolving under relaxed selection in the LTEE. In 5 out of 6 nonmutator populations (top two rows), the trajectory of this gene set falls within the null distribution. The remaining nonmutator population, Ara+5, has no mutations in this gene set, and so falls significantly below the null distribution (two-tailed bootstrap: Bonferroni-corrected $p < 0.005$). In 5 out of 6 hypermutator populations (bottom two rows), the trajectory of this gene set falls within the null distribution. The remaining hypermutator population, Ara+6 lies at the margin of the null distribution (two-tailed bootstrap: Bonferroni-corrected $p = 0.06$). Supplementary Figure S1 shows the result of applying STIMS on these genes, summed across all 12 LTEE populations. Overall, the global tempo of observed mutations in the nonmutator populations is best explained by the occurrence and fixation of beneficial mutations with small numbers of hitchhikers. By contrast, the global tempo of observed mutations in the hypermutator populations is best explained by large numbers of nearly neutral mutations hitchhiking to high frequency with a much smaller number of beneficial mutations [15].

Control 2: Detecting purifying selection in the LTEE

As a second control, we examined genes that were experimentally shown to be essential or nearly essential in REL606 under LTEE conditions [6]. Many of the genes under strongest positive selection in the LTEE are also essential genes [23]. Thus, we excluded 24 essential genes with evidence of parallel evolution in the LTEE (Materials and Methods). We hypothesized that the remaining 491 essential genes would show evidence of purifying selection in the hypermutator populations, such that those loci would be depleted in mutations in comparison to the null distribution (Figure 6 and Supplementary Figure S2). Indeed, these 491 loci show significant depletion of observed mutations in all 6 hypermutator populations (one-tailed bootstrap: $p < 0.0001$ for Ara−1; $p < 0.01$ for Ara−2; $p < 0.01$ for Ara−3; $p < 0.005$ for Ara−4; $p < 0.02$ for Ara+3; $p < 0.0001$ for Ara+6). Additionally, one of the six nonmutator populations, Ara+1 shows a marginally significant depletion of mutations at these loci (one-tailed bootstrap: $p < 0.05$). Ara+1 evolved a insertion-sequence hypermutator phenotype early in

194 its evolutionary history [30-32], so it is plausible that signatures of purifying selection can be
195 seen in Ara+1 [25], even though it did not evolve an elevated point-mutation rate [31].
196 Despite the global signal of purifying selection on these 491 essential genes, it is not clear
197 which specific ones are under purifying selection. The best candidates are the ones that have no
198 mutations whatsoever in the LTEE, while the second-best are those that were only affected by
199 synonymous mutations. We found 65 genes with no observed mutations in the metagenomics
200 data, 18 of which are essential. 105 genes have only synonymous mutations, 30 of which are
201 essential. We examined 491 essential genes, out of 3948 genes in the genome that passed our
202 filters (Materials and Methods). Based on these numbers, there is a significant association
203 between essentiality and having no observed mutations (Fisher's exact test: $p = 0.0007$) and
204 between essentiality and only having synonymous mutations (Fisher's exact test: $p < 10^{-5}$). The
205 first set of candidates for purifying selection in the LTEE are reported in Supplementary Table
206 S1, and the second set of candidates are reported in Supplementary Table S2. As one would
207 expect, many of these genes encode proteins that catalyze key biological reactions, such as ATP
208 synthase and ribosomal proteins.
209
210 *Control 3: Verifying positive selection in the LTEE*
211 As a final control, we examined genes that have previously been shown to be evolving
212 under positive selection in the LTEE. We examined the genes with the strongest signal of
213 parallel evolution in genomes sampled over the first 50,000 generations of the LTEE [15].
214 We first considered the 50 genes with the most parallelism in the nonmutator populations
215 (Figure 7 and Supplementary Figure S3). STIMS recovered the expected signal of positive
216 selection on these genes in the nonmutator populations (one-tailed bootstrap: $p < 0.0001$ in all
217 cases). STIMS also found an overall signal of positive selection on these genes in the
218 hypermutator populations (one-tailed bootstrap: $p < 0.05$ in all hypermutator populations).
219 In the same fashion, we examined the genes with the strongest signal of parallel evolution
220 in the hypermutator genomes (Supplementary Figure S4 and Supplementary Figure S5). The
221 nonmutator populations accumulate mutations in this gene set at a rate similar to background. As
222 expected, 5 out 6 hypermutator populations show a strong excess of mutations above background
223 (one-tailed bootstrap: $p < 0.02$ in Ara−1, Ara−2, Ara−4, Ara+3, Ara+6). In the remaining
224 population, Ara−3, mutations in this gene set accumulate at the background rate. It is unclear

why this population is an outlier, but this finding may be related to the evolution of a citrate metabolic innovation that modified the ecology of this population [33].

Comparison of STIMS to a test for selection based on the Poisson distribution

We also benchmarked STIMS against a statistical test for selection that uses the Poisson distribution to model the expected distribution of mutations per genomic site per unit time under neutral evolution [16, 34]. In brief, STIMS trades off sensitivity for higher specificity (lower false positive rate) in comparison to the Poisson method, and also has the advantage of showing how the tempo of molecular evolution varies over time in a gene set of interest. These findings, and additional considerations, are described in detail in the Supplementary Text.

Application to module decompositions of the E. coli genome

Our control experiments demonstrate that STIMS is capable of recovering signals of purifying and positive selection. In this section, we use STIMS to examine how different modules of genes in the *E. coli* genome are evolving in the LTEE. Our goal is to develop testable hypotheses for which genetic modules and biochemical pathways underlie the ongoing fitness gains observed in the LTEE [35]. We examined three different module decompositions of the *E. coli* genome. The first partitioned the *E. coli* proteome into sectors based on quantitative mass spectrometry [26]; the second reported sets of genes ("eigengenes") whose expression best predicted *E. coli* growth rates [28]; while the third partitioned the gene regulatory network into independent components based on gene expression [27].

<u>Two proteome sectors show evidence of purifying selection.</u> We examined proteome sectors that were identified by quantitative mass spectroscopy during carbon-, nitrogen-, and ribosome-limiting growth conditions [26]. Supplementary Figure S6 shows our findings. One proteome sector was significantly depleted in mutations in Ara−1, Ara+3, and Ara+6, suggesting purifying selection, and also shows evidence of positive selection in Ara+5. This one, called the U-sector (green), contains genes that were not upregulated by any of the growth-limitation treatments in [26]. Rather, the expression of the proteins in the U-sector show a generic positive correlation with growth rate across all of the conditions tested by Hui et al. [26]. When STIMS is applied to these modules, considering mutations summed across *all* LTEE populations, we also see an overall depletion of mutations in proteins in the R-sector (yellow; Supplementary Figure

256 S7). Proteins in the R-sector are upregulated under ribosome-limiting growth conditions, and are
257 associated with translation [26].
258 No evidence of selection on *E. coli* eigengenes. Finally, we examined the sets of genes
259 (called eigengenes), that were most predictive of *E. coli's* growth rate (and presumably fitness
260 under LTEE conditions), using different *E. coli* strains and growth environments [28]. No
261 eigengenes showed any evidence of selection in the LTEE (Supplementary Figure S8 and S9).
262 Regulators of I-modulons are under positive selection. Sastry et al. (2019) used
263 independent component analysis on the *E. coli* transcriptome, sampled across diverse conditions
264 and strains, to infer 92 independent modules (called I-modulons) in the *E. coli* gene regulatory
265 network (GRN). 61 of the 92 I-modulons correspond to known transcription factors and
266 regulators in the GRN. We asked two questions: first, is there a difference between how the
267 regulators and regulated genes in the I-modulons evolve in the LTEE? Second, are any I-
268 modulons enriched with or depleted of mutations in the LTEE?
269 We find that transcriptional regulators of the I-modulons are under strong positive
270 selection in the LTEE, while the genes within I-modulons are under much weaker selection
271 (Figure 8). In all 12 populations, regulators of I-modulons are under stronger selection than the
272 genes in the I-modulons themselves. I-modulon regulators are under very strong selection in all 6
273 nonmutator populations (one-tailed bootstrap: $p < 0.001$ in all nonmutator populations), and
274 show evidence of ongoing positive selection in some hypermutator populations as well (one-
275 tailed bootstrap: $p = 0.03$ in Ara−3, $p \leq 0.0001$ in Ara+3 and Ara+6). By contrast, the evolution
276 of genes within I-modulons fits the null distribution in most populations, although Ara−4 and
277 Ara+3 show evidence of purifying selection. When mutations across all LTEE populations are
278 considered, genes regulated within I-modulons show an overall signal of purifying selection
279 (Supplementary Figure S10). Together, these results indicate that the upper levels of the
280 regulatory hierarchy of the *E. coli* GRN are under strong selection in the LTEE, while the
281 effector genes at the lower levels of the gene regulatory hierarchy are under weaker selection.
282 Figure 8 also shows that the tempo of I-modulon regulator evolution is quite variable
283 across populations. Consider the number of mutations in I-modulon regulators in the nonmutator
284 populations. After 40,000 generations, Ara+1 has 5, Ara+2 has 4, Ara+4 has 2, and Ara+5 has 1,
285 while Ara−5 and Ara−6 have none. Variation in the tempo of evolution of I-modulon regulators

286 is also seen in the hypermutator populations, in particular the strong signal of ongoing positive
287 selection found in Ara+3 and Ara+6, in contrast with the complete lack of signal in Ara−4.
288 While I-modulons tend to evolve at background rates within individual populations
289 (Figure 8), some specific I-modulons show evidence of idiosyncratic selection in the
290 hypermutator populations. We hypothesize that some of these cases represent historical
291 contingency and epistasis in the LTEE; these hypotheses could be tested in future studies. The
292 results for all I-modulons are provided in Supplementary Files 1 and 2, while particular I-
293 modulons of interest are listed in Supplementary Table 3.
294
295 Summary of module decomposition results. Altogether, we find that the protein-coding
296 genes with the strongest transcriptional response to changing conditions show little to no
297 evidence of selection in the LTEE. By contrast, top-level transcriptional regulators showed
298 strong signatures of positive selection in all nonmutator populations, as well as in some
299 hypermutator populations. Based on these findings, we hypothesize that the genes that show the
300 strongest transcriptional response to changing conditions tend to be at the lower levels of the
301 gene regulatory network, while natural selection in the LTEE is largely operating on regulators
302 of those genes.
303
304 Cis-*regulatory regions of key regulators show significantly more parallel evolution than the cis-*
305 *regulatory regions of downstream targets*
306 If upper levels of the gene regulatory network are under stronger selection in the LTEE,
307 then *cis*-regulatory regions of I-modulon regulators should also show more evidence of positive
308 selection than the genes within I-modulons. We tested this prediction by examining non-coding
309 mutations associated with I-modulon regulators and their downstream targets. These non-coding
310 mutations occurred within the promoter regions (up to 100 bp upstream) of their annotated gene
311 [16]. There are 48 non-coding mutations associated with 70 I-modulon regulators, and 542 non-
312 coding mutations associated with 1394 genes regulated within I-modulons. These data are
313 consistent with our prediction (Binomial test with 48 successes out of 590 trials and expected
314 probability of success = 70/1464: $p = 0.0005$).
315

316 *Application of STIMS to hypermutator populations of* Pseudomonas aeruginosa *evolving under*
317 *antibiotic selection*
318 We wanted to know whether STIMS could be applied beyond the LTEE. Unlike the
319 LTEE, however, most evolution experiments do not have genomic, let alone metagenomic, data
320 spanning 30+ years of evolutionary history. We sourced the metagenomic time series data
321 reported by Mehta et al. [8], in which replicate populations of *Pseudomonas aeruginosa* adapted
322 to subinhibitory concentrations of colistin in continuous chemostat culture for one month. We
323 reasoned that the Mehta dataset would be ideal for applying STIMS since both replicate
324 populations in that experiment rapidly evolved hypermutator phenotypes. We asked whether
325 annotated regulatory genes in the *P. aeruginosa* PAO11 genome showed evidence of positive
326 selection in this evolution experiment (Figure 9, Supplementary Figure S11); indeed, STIMS
327 reveals a clear signal of positive selection on the pre-specified set of 424 regulatory genes (one-
328 tailed bootstrap: $p < 0.001$). This finding reveals that STIMS has the power to detect gene sets
329 under strong positive or purifying selection, even when applied to metagenomic time series
330 which span relatively short time periods.
331
332
333 **DISCUSSION**
334
335 We show that signals of both positive and purifying selection can be detected in
336 metagenomic time series of large asexual haploid populations, including *Escherichia coli* from
337 Lenski's long-term evolution experiment (LTEE) and a clinically relevant pathogen,
338 *Pseudomonas aeruginosa*, in a short-term evolution experiment under antibiotic selection.
339 In contrast to previous studies, which examined global patterns in the tempo and mode of
340 evolution in the LTEE [13, 15, 16], our analysis focuses on functional modules encoded by the
341 *E. coli* genome. We find that the tempo of evolution in particular molecular subsystems gives us
342 insight into the mode of evolution acting on those modules (i.e., relaxed, purifying, or positive
343 selection). We ran simulations to demonstrate that STIMS works in an idealized system in which
344 selection pressures and the genomic DFE can be pre-specified *a priori*, and we ran
345 computational positive control experiments to confirm that STIMS works on genes with prior
346 evidence of relaxed (Figure 5), purifying (Figure 6), and positive selection (Figure 7).

347 Our findings indicate that the accelerated pace of genomic evolution in the
348 hypermutators, combined with the detailed record of molecular evolution provided by
349 metagenomic time series, may open new opportunities for understanding the genomic basis of
350 adaptive evolution, even though the signal of selection is obscured in hypermutator genomes due
351 to genomic draft [6]. First, the vast number of nearly neutral hitchhikers that are observed in
352 hypermutator populations provides insight into how mutations in modifier alleles affect genome-
353 wide and local mutation rates and biases [31]. Second, regions of the genome that are highly
354 depleted in mutations in the hypermutator populations are strong candidates for purifying
355 selection. Third and most importantly— metagenomic sequencing gives deep sampling of
356 genetic variation off the (eventual) line of descent.
357 We found compelling evidence of purifying selection in the hypermutator populations of
358 the LTEE. Many of the strongest candidate genes for purifying selection are deeply conserved
359 over evolutionary time, such as those encoding ribosomal subunits. The action of purifying
360 selection on the hypermutator populations is also consistent with the observation that antimutator
361 alleles have fixed in several populations of the LTEE [31, 36], and with the experimental finding
362 that overexpressing RNA chaperones in some hypermutator LTEE strains reduces the mutation
363 load in those strains [37]. Together, these observations suggest that hypermutator lineages are
364 accumulating some deleterious passenger mutations, even as their fitness continues to increase.
365 In any case, our analysis shows that the depletion of mutations in particular genes is not due to
366 the evolution of antimutator alleles: by bootstrapping a null distribution of background rates,
367 STIMS controls for the genome- and population-wide effects of antimutator alleles over time.
368 The resampling approach used by STIMS can also take the effects of local mutation
369 biases into account [38]. For instance, one can control for local mutation biases by constructing
370 null distributions that directly model chromosomal variation in mutation rates and biases. This
371 can be somewhat complicated, given that mutational biases [6] and regional mutation rates over
372 the chromosome have evolved idiosyncratically across the replicate LTEE populations [31]. Our
373 implementation of STIMS samples gene sets uniformly over the *E. coli* genome: we also
374 implemented a sampling procedure that take the wave pattern of mutation rate variation over the
375 *E. coli* chromosome into account [31, 39, 40], but this more complicated procedure produced the
376 same results as sampling genes uniformly over the chromosome (Materials and Methods).

When we applied STIMS to different module decompositions of the *E. coli* genome, we found compelling evidence of strong positive selection on key global regulators of the *E. coli* gene regulatory network, especially in comparison to the genes that they regulate. Furthermore, we found an excess of mutations in the *cis*-regulatory regions of those regulators in comparison to the genes that they regulate. One explanation could be that mutations that affect the *cis*-regulation and structure of global regulators at higher levels of the GRN cause a cascade of effects on downstream targets, and so are more effective targets for fine-tuning the *E. coli* GRN. Strikingly, we found evidence of continued strong positive selection on key regulatory genes in the two populations with the most mutations in the LTEE: Ara+3 and Ara+6 (Figure 8). By contrast, two nonmutator populations, Ara−5 and Ara−6, showed no mutations at all in I-modulon regulators in the last 20,000 generations of the time course. This suggests that the GRN may initially evolve close to some local fitness maximum (subject to pleiotropic constraints), but then evolve further to compensate for the effects of mutations elsewhere in the genome.

Further work will be needed to test the hypothesis that ongoing evolution of I-modulon regulators is related to compensatory evolution. It is possible that the hypermutator populations are evolving to compensate for an increasing mutation load of deleterious hitchhiker mutations [8]. The appearance of multiple antimutator alleles in the LTEE suggests that that hypermutability has a hidden cost [15, 31, 36], but the magnitude of any mutation load in the LTEE populations remains unknown. Ongoing positive selection on the *E. coli* GRN could also be due to compensatory evolution that is not specifically for hitchhiking deleterious mutations. For instance, it is possible that early beneficial mutations become deleterious due to further mutations [41, 42]. Furthermore, natural selection may greedily favor mutationally accessible but suboptimal trajectories [43, 44] that then open new, idiosyncratic paths for further refinement [45].

Our work has some limitations. By using STIMS to examine the tempo of GRN evolution in the LTEE using the same dataset, we find a number of patterns with an unknown rate of false positives. Therefore, future work is needed to test the specific hypotheses that we have generated, either by using additional time-course data from the LTEE, by analyzing related evolution experiments, or by experimental validation. An important caveat is that deletions that fix in the LTEE can lead to spurious inferences of purifying selection, if they are not taken into account, since deleted genes cannot accumulate mutations. By that same token, gene

408 duplications, amplifications, or other forms of copy number variation could lead to spurious
409 inferences of positive selection, or elevated mutation rates [46, 47]. Those types of mutations
410 appear to be rare in these data, in comparison to the point mutations, indels, and transposon
411 insertions that we count. The complications induced by copy number variation may need to be
412 considered (or safely ignored), depending on the context in which STIMS is used. Finally,
413 STIMS is computationally intensive due to its use of bootstrapping. Often equivalent statistical
414 results can be derived much faster, using exact tests like the binomial test or Fisher's exact test
415 [8], or by using tests based on the Poisson distribution [34, 48]. The advantage of STIMS is that
416 it provides greater biological insight, by visualizing *how* statistical signatures of positive and
417 purifying selection change in an evolving population over time.
418 Overall, our work provides greater insight into the mechanistic connection between
419 genotypic and phenotypic evolution in evolution experiments like the LTEE. The genetic
420 architecture underlying fitness improvements in the LTEE likely involves a relatively small
421 number of loci that control global aspects of cellular physiology [15, 16, 23, 49]. These factors
422 may control many downstream pathways, which are being modulated in response to selection in
423 the LTEE. Hence, we hypothesize that the regulation of these pathways is being rewired during
424 the LTEE, often without significantly changing their downstream effectors. This would explain
425 why the modules that show the strongest changes in expression, and best predict growth rate and
426 fitness in response to environmental conditions [26-28] show little evidence of adaptive
427 evolution in the LTEE. Overall, the genotype-phenotype map of *E. coli*, at least in the context of
428 the LTEE, resembles the hierarchical "supervisor-worker" gene architecture proposed by Chen et
429 al. [50] to explain the genetic architecture of quantitative traits in *Saccharomyces cerevisiae*.
430 As the costs of protein production exerts a strong contrast on cellular energetics, the
431 proper allocation of proteome resources in order to maximize growth, rather the evolution of
432 particular genetic modules, may be the cellular phenotype under strongest selection in the LTEE
433 [51-54]. Future work could test this hypothesis by trying to mimic evolutionary changes in the
434 LTEE by directly perturbing the balance of global physiological and metabolic state variables
435 (chromosome conformation, ppGpp, cAMP levels and redox potential) to maximize growth in
436 the ancestral REL606 strain. Coevolution between the function of those proteome resources,
437 pleiotropic constraints on optimal allocation, as well as feedback with the environment could all
438 play a part in causing the open-ended increases in fitness seen in the LTEE [20, 35].

439 Finally, we expect our methodology will be broadly useful, especially for workers in the
440 experimental evolution field. To demonstrate the generality of STIMS, we reanalyzed data from
441 a second evolution experiment in which two replicate hypermutator populations of *P. aeruginosa*
442 adapted to subinhibitory concentrations of colistin [8]. Our finding of positive selection on
443 regulatory genes in this experiment validates STIMS as a general method and indicates that the
444 rapid evolution of bacterial gene regulatory networks may be a general mechanism for adaptation
445 during experimental evolution, and perhaps during adaptation to novel environments in general.
446 We expect that our basic idea could be more rigorously justified by deeper theoretical work, and
447 further extended to study evolving populations and communities in both the laboratory and in the
448 wild. Purifying selection is of particular interest in the study of viruses and cancers, for the sake
449 of finding conserved and effective drug targets [55-58]. In particular, we anticipate that STIMS
450 could be applied to clinical time series, such as genomic sampling from cystic fibrosis patients
451 [59, 60], in order to discover gene modules that are under selection in pathogens as they adapt to
452 their host [61, 62].
453
454 **MATERIALS AND METHODS**
455
456 *The STIMS algorithm*
457 In brief, STIMS counts the cumulative number of mutations occurring over time in a
458 module of interest, and compares that number to a null distribution that is constructed by
459 subsampling random sets of genes over the genome, in which the cardinality of these random
460 gene sets is fixed to the cardinality of the module of interest. We normalize the number of
461 observed mutations in a gene set by the total length of that gene set in base-pairs.
462 In this work, we specifically counted point mutations, small insertions and deletions
463 (indels), and transposon insertions (structural variants) that were detected in metagenomic time
464 series using the *breseq* pipeline [8, 16, 63]. Nonetheless, STIMS does not depend on any specific
465 variant calling software, nor does it specifically require metagenomic time series (genomic time
466 series would suffice). STIMS only requires a list of observed *de novo* mutations over time (i.e.
467 information about the location of each mutation, and the time at which each was first observed in
468 the population).

469 By bootstrapping a null distribution based on random gene sets, STIMS implicitly
470 controls for genome-wide variation in the mutation rate (since this will affect all genes). In order
471 to control for local variations in mutation rate [31, 39, 40], we subsampled random modules from
472 the same chromosomal neighborhood as the module of interest (dividing the REL606 genome
473 into 46 bins, roughly ~100,000 bp each), under the assumption that nearby genes have similar
474 mutation rates. This approach gave the same results as sampling genes uniformly across the
475 genome, despite a higher computational cost. For this reason, the results reported here use the
476 simplest method to construct the null distribution, in which genes are sampled without
477 considering their position on the chromosome.
478 Bootstrapped *p*-values were calculated separately for each population. *p*-values for one-
479 sided tests are exact estimates of the relevant tail of the null distribution, where *p* is the upper-tail
480 (or lower-tail) probability of the event of sampling a normalized cumulative number of mutations
481 under the null distribution that is greater than (or less than) the normalized cumulative number of
482 mutations of the module of interest. Two-tailed tests against the bootstrapped null distribution
483 were calculated with a false-positive (type I error) probability $\alpha = 0.025$ to account for both tails;
484 this is equivalent to multiplying *p*-values by a factor of 2, in a Bonferroni correction for two
485 statistical tests (i.e., on the upper tail and on the lower tail of the null distribution).
486 In the visualizations shown in the figures, the top 2.5% and bottom 2.5% of points in the
487 null distribution are omitted, such that each panel can be directly interpreted as a randomization
488 test with a false-positive (type I error) probability $\alpha = 0.05$.
489
490 *Filtering of genes in REL606 genome*
491 We analyzed the pre-processed LTEE metagenomics data published by [16], and so we
492 applied filters to exclude regions of the REL606 genome that were omitted from that analysis. In
493 particular, pseudogenes and genes in repetitive regions of the genome were excluded. A site was
494 marked as repetitive if (1) it was annotated as a repeat region in the REL606 reference, (2) it was
495 present in the set of masked regions compiled by [15], or (3) it fell within the putative prophage
496 at REL606 genome coordinates 880528–904682.
497
498 *Essential genes excluded from purifying selection control experiment*

499 We excluded essential genes that showed parallel evolution in Tenaillon et al. [15]. In
500 that work, a G-score was calculated to measure parallel evolution. G-scores were calculated
501 separately for the nonmutator and hypermutator populations. We ranked all genes in REL606
502 that passed our filters by their nonmutator and hypermutator G-scores. Essential genes that were
503 in the top 50 of either list were excluded from the purifying selection control experiment. 21 out
504 of the top 50 G-scoring nonmutator genes were essential in REL606, based on the transposon
505 mutagenesis and sequencing experiments carried out by Couce et al. [6]. These genes were:
506 *arcA*, *arcB*, *crp*, *fabF*, *ftsI*, *hflB*, *infB*, *infC*, *mrdA*, *mreB*, *mreC*, *mreD*, *nusA*, *rne*, *rplF*, *rpoB*,
507 *rpsD*, *sapF*, *spoT*, *topA*, and *yabB*. 3 out of the top 50 G-scoring hypermutator genes were
508 essential in REL606. These genes were: *sapA*, *tilS*, and *yhbH*.
509
510 *Analysis of regulatory genes in the month-long hypermutator P. aeruginosa evolution experiment*
511 We analyzed the pre-processed metagenomics data from the hypermutator *P. aeruginosa*
512 evolution experiment published by Mehta et al. [8]. We excluded the Pf4 bacteriophage in the *P.*
513 *aeruginosa* PAO11 reference genome used by Mehta et al. from the STIMS analysis; this region
514 was also omitted from the statistical analysis in the original report [8].
515 We used the keywords "regulator", "regulatory", and "regulation" to search for
516 regulatory genes in the PAO11 genome to identify *de novo* mutations arising in their evolution
517 experiment. This search resulted in a set of 424 regulatory genes, which we then analyzed using
518 STIMS.
519
520 *Implementation of a test for selection based on the Poisson distribution*
521 We implemented the Poisson method described by Kinnersley et al. [34]. We summed all
522 mutations across the LTEE associated with genes that passed our filters, and divided by the total
523 length of those genes to calculate the background density of mutations per site, λ. For each gene
524 g in the genome, we scale λ by the length of g, to calculate the expected number of mutations at
525 gene g: λ_g. The same calculation holds for a set of genes: by multiplying λ by the total length of
526 genes in the set, we can calculate the expected number of mutations in the gene set, λ_{set}. Suppose
527 x mutations were counted in the gene set of interest. Then, a one-tailed test for purifying
528 selection in this gene set can be done by calculating a p-value from the lower-tail of the Poisson

529 distribution: $P(X \leq x) = \sum_{k=0}^{k=x} \frac{\lambda_{set}^{k}}{k!} e^{-\lambda_{set}}$. Similarly, a one-tailed test for positive selection in
530 the gene set can be done by directly calculating a *p*-value from the upper-tail of the Poisson
531 distribution:
532 $P(X \geq x) = \sum_{k=x}^{k=\infty} \frac{\lambda_{set}^{k}}{k!} e^{-\lambda_{set}}$. When multiple genes or gene sets were tested for positive or
533 purifying selection, we applied a Benjamini-Hochberg correction for multiple-testing, and report
534 those false-discovery-rate (FDR) corrected *p*-values.
535
536 *Wright-Fisher simulations of microbial evolution*
537 We implemented Wright-Fisher evolutionary simulations of asexual haploid populations
538 in SLiM [64]. We simulated populations of 1 million cells, each containing a genome of 1,000
539 contiguous genes. We tested STIMS in two scenarios: the evolution of a nonmutator populations
540 with a point-mutation rate of 10^{-10} per base-pair per generation, and the evolution of a
541 hypermutator populations with a 100-fold increase in mutation rate: 10^{-8} per base-pair per
542 generation. These population genetic parameters are comparable to the effective population size
543 (3.3×10^{7}) and the ancestral mutation rate (8.9×10^{-11}) of Lenski's LTEE [29], and the 100-fold
544 evolved increases in mutation rates observed in the LTEE [31]. Our simulations assume a
545 background genomic distribution of mutation fitness effects (DFE) in which the vast majority of
546 mutations are nearly neutral, with a long tail of deleterious mutations, based on high-throughput
547 measurements of the DFE in *E. coli* in microfluidic mutation accumulation experiments [65]. We
548 assume that 100 genes are evolving under positive selection, such that 10% of mutations
549 occurring in those genes are beneficial. This assumption implies that 0.0025 of mutations are
550 beneficial in our model, which is comparable to the experimental estimate that 1 out of 150
551 newly arising mutations in *E. coli* are beneficial in laboratory conditions [66]. Following recent
552 simulations of adaptive evolution in the LTEE, we draw beneficial mutations from an
553 exponential DFE with mean 0.01578 [29]. We further assume that 100 genes are evolving
554 completely neutrally such that mutations in these genes have no fitness effect, and assume that
555 another set of 100 genes are evolving under purifying selection, such that 40% of mutations in
556 those genes cause a 30% decrease in fitness. This last assumption matches the finding that 1% of
557 new mutations in *E. coli* are lethal under laboratory conditions [65].

558 Ten replicate simulations were run for both the nonmutator and hypermutator
559 populations, and all mutations in each simulation were saved at 100-generation intervals.
560 Mutations were filtered based on a 1% allele frequency threshold, to simulate metagenomic
561 sequencing: this is equivalent to uniform 100× short-read sequencing coverage across the
562 genome per sequencing sample, with no sequencing errors. We then ran STIMS on the 100 genes
563 under positive selection, the 100 genes under relaxed selection (those evolving completely
564 neutrally), and the 100 genes under purifying selection. We examined the sensitivity and
565 specificity of STIMS by varying the allele frequency detection threshold, the number of genes
566 sampled per module, the sampling interval in the time series, and the length of the time series,
567 holding all other setting to their default values. Four values of the allele frequency detection limit
568 were examined: 0.01%, 1%, 5%, 10%. The number of genes sampled per module was varied
569 between 1, 25, 50, and 100 genes. The sampling interval was either 100- or 500-generation
570 intervals. The length of the time series was 500, 1000, 2000, or 5000 generations. True positives
571 and false negatives were counted by the number of STIMS tests on the genes evolving under
572 positive or purifying selection that passed a one-sided *p*-value significance threshold of 0.05.
573 False positives and true negatives were counted by the number of STIMS tests on the genes
574 evolving neutrally that nevertheless passed the same *p*-value significance threshold. Sensitivity
575 (also known as the true positive rate, or as statistical power) was calculated as the number of true
576 positives divided by the sum of true positives and false negatives, out of the 10 tests on the 10
577 replicate datasets. Specificity (also known as the true negative rate) was calculated as the number
578 of true negatives divided by the sum of true negatives and false positives, out of the 10 tests on
579 the 10 replicate datasets.
580
581 *Data and analysis code availability*
582 All analysis codes for this project are available at:
583 www.github.com/rohanmaddamsetti/LTEE-purifying-selection. A stand-alone implementation of
584 STIMS in the Julia programming language is available at:
585 www.github.com/rohanmaddamsetti/STIMS. The sequence data used in our study have already
586 been deposited into a public database. The other data and analysis scripts in this manuscript have
587 been archived on the Zenodo Digital Repository (DOI: http://doi.org/10.5281/zenodo.4783368).
588

589 **ACKNOWLEDGEMENTS**

590 We thank Alejandro Couce for sharing the list of gold-standard neutral genes in *E. coli* B strain
591 REL606. We thank Richard Lenski for valuable discussions and advice. We thank Jeffrey
592 Barrick for valuable discussions, advice, and comments on an earlier version of our manuscript.
593 We also thank Benjamin Good for making pre-processed LTEE metagenomic data and analysis
594 scripts accessible for the research community. The LTEE that generated the bacteria we used in
595 this study is supported by a grant from the National Science Foundation (currently DEB-
596 1951307) to Richard Lenski and Jeffrey Barrick. N.A.G. was supported in part by the BEACON
597 Center for the Study of Evolution in Action (NSF cooperative agreement DBI-0939454) and by
598 Michigan State University.

599

600

601 **REFERENCES**

602

603 1. Jeggo PA, Pearl LH, Carr AM. DNA repair, genome stability and cancer: a historical
604 perspective. Nature Reviews Cancer. 2016;16(1):35.

605 2. Loeb LA. A mutator phenotype in cancer. Cancer research. 2001;61(8):3230-9.

606 3. Modrich P. Mismatch repair, genetic stability, and cancer. Science.
607 1994;266(5193):1959-61.

608 4. Feliziani S, Marvig RL, Lujan AM, Moyano AJ, Di Rienzo JA, Johansen HK, et al.
609 Coexistence and within-host evolution of diversified lineages of hypermutable Pseudomonas
610 aeruginosa in long-term cystic fibrosis infections. PLoS Genet. 2014;10(10):e1004651.

611 5. Ford CB, Shah RR, Maeda MK, Gagneux S, Murray MB, Cohen T, et al. Mycobacterium
612 tuberculosis mutation rate estimates from different lineages predict substantial differences in the
613 emergence of drug-resistant tuberculosis. Nature genetics. 2013;45(7):784-90.

614 6. Couce A, Caudwell LV, Feinauer C, Hindré T, Feugeas J-P, Weigt M, et al. Mutator
615 genomes decay, despite sustained fitness gains, in a long-term experiment with bacteria.
616 Proceedings of the National Academy of Sciences. 2017;114(43):E9026-E35.

617 7. Schiffels S, Szöllősi GJ, Mustonen V, Lässig M. Emergent neutrality in adaptive asexual
618 evolution. Genetics. 2011;189(4):1361-75.

619 8. Mehta HH, Prater AG, Beabout K, Elworth RA, Karavis M, Gibbons HS, et al. The
620 essential role of hypermutation in rapid adaptation to antibiotic stress. Antimicrobial agents and
621 chemotherapy. 2019;63(7):e00744-19.

622 9. Hammerstrom TG, Beabout K, Clements TP, Saxer G, Shamoo Y. Acinetobacter
623 baumannii repeatedly evolves a hypermutator phenotype in response to tigecycline that
624 effectively surveys evolutionary trajectories to resistance. PloS one. 2015;10(10):e0140489.

625 10. Lenski RE, Rose MR, Simpson SC, Tadler SC. Long-term experimental evolution in
626 Escherichia coli. I. Adaptation and divergence during 2,000 generations. The American
627 Naturalist. 1991;138(6):1315-41.

628 11. Lenski RE. Experimental evolution and the dynamics of adaptation and genome
629 evolution in microbial populations. The ISME journal. 2017;11(10):2181-94.

630 12. Barrick JE, Lenski RE. Genome-wide mutational diversity in an evolving population of
631 Escherichia coli. Cold Spring Harbor symposia on quantitative biology. 2009;74:119-29.

632 13. Barrick JE, Yu DS, Yoon SH, Jeong H, Oh TK, Schneider D, et al. Genome evolution
633 and adaptation in a long-term experiment with Escherichia coli. Nature. 2009;461(7268):1243-7.

634 14. Maddamsetti R, Lenski RE, Barrick JE. Adaptation, clonal interference, and frequency-
635 dependent interactions in a long-term evolution experiment with Escherichia coli. Genetics.
636 2015;200(2):619-31.

637 15. Tenaillon O, Barrick JE, Ribeck N, Deatherage DE, Blanchard JL, Dasgupta A, et al.
638 Tempo and mode of genome evolution in a 50,000-generation experiment. Nature.
639 2016;536(7615):165-70.

640 16. Good BH, McDonald MJ, Barrick JE, Lenski RE, Desai MM. The dynamics of molecular
641 evolution over 60,000 generations. Nature. 2017;551(7678):45-50.

642 17. Vasi F, Travisano M, Lenski RE. Long-term experimental evolution in Escherichia coli.
643 II. Changes in life-history traits during adaptation to a seasonal environment. The american
644 naturalist. 1994;144(3):432-56.

645 18. Lenski RE, Mongold JA, Sniegowski PD, Travisano M, Vasi F, Gerrish PJ, et al.
646 Evolution of competitive fitness in experimental populations of E. coli: what makes one
647 genotype a better competitor than another? Antonie van Leeuwenhoek. 1998;73(1):35-47.

648 19. Elena SF, Cooper VS, Lenski RE. Punctuated evolution caused by selection of rare
649 beneficial mutations. Science. 1996;272(5269):1802-4.

650 20. Wiser MJ, Ribeck N, Lenski RE. Long-term dynamics of adaptation in asexual
651 populations. Science. 2013;342(6164):1364-7.

652 21. Grant NA, Maddamsetti R, Lenski RE. Maintenance of metabolic plasticity despite
653 relaxed selection in a long-term evolution experiment with Escherichia coli. The American
654 Naturalist. 2021;0(ja):null. doi: 10.1086/714530.

655 22. Grant NA, Magid AA, Franklin J, Dufour Y, Lenski RE. Changes in Cell Size and Shape
656 During 50,000 Generations of Experimental Evolution with Escherichia coli. Journal of
657 Bacteriology. 2021;203(10).

658 23. Maddamsetti R, Hatcher PJ, Green AG, Williams BL, Marks DS, Lenski RE. Core genes
659 evolve rapidly in the long-term evolution experiment with Escherichia coli. Genome biology and
660 evolution. 2017;9(4):1072-83.

661 24. Maddamsetti R. Universal constraints on protein evolution in the long-term evolution
662 experiment with Escherichia coli. Genome Biology and Evolution. 2021. doi:
663 10.1093/gbe/evab070.

664 25. Maddamsetti R. Selection maintains protein interactome resilience in the long-term
665 evolution experiment with Escherichia coli. Genome Biology and Evolution. 2021. doi:
666 10.1093/gbe/evab074.

667 26. Hui S, Silverman JM, Chen SS, Erickson DW, Basan M, Wang J, et al. Quantitative
668 proteomic analysis reveals a simple strategy of global resource allocation in bacteria. Molecular
669 systems biology. 2015;11(2).

670 27. Sastry AV, Gao Y, Szubin R, Hefner Y, Xu S, Kim D, et al. The Escherichia coli
671 transcriptome mostly consists of independently regulated modules. Nature communications.
672 2019;10(1):1-14.

673 28. Wytock TP, Motter AE. Predicting growth rate from gene expression. Proceedings of the
674 National Academy of Sciences. 2019;116(2):367-72.

675 29. Izutsu M, Lake DM, Matson ZW, Dodson JP, Lenski RE. Effects of periodic bottlenecks
676 on the dynamics of adaptive evolution in microbial populations. bioRxiv. 2021.

677 30. Papadopoulos D, Schneider D, Meier-Eiss J, Arber W, Lenski RE, Blot M. Genomic
678 evolution during a 10,000-generation experiment with bacteria. Proceedings of the National
679 Academy of Sciences. 1999;96(7):3807-12.

680 31. Maddamsetti R, Grant NA. Divergent evolution of mutation rates and biases in the long-
681 term evolution experiment with Escherichia coli. Genome Biology and Evolution. 2020. doi:
682 10.1093/gbe/evaa178.

683 32. Consuegra J, Gaffé J, Lenski RE, Hindré T, Barrick JE, Tenaillon O, et al. Insertion-
684 sequence-mediated mutations both promote and constrain evolvability during a long-term
685 experiment with bacteria. Nature communications. 2021;12(1):1-12.

686 33. Turner CB, Blount ZD, Mitchell DH, Lenski RE. Evolution and coexistence in response
687 to a key innovation in a long-term evolution experiment with Escherichia coli. bioRxiv.
688 2015:020958.

689 34. Kinnersley M, Schwartz K, Yang D-D, Sherlock G, Rosenzweig F. Evolutionary
690 dynamics and structural consequences of de novo beneficial mutations and mutant lineages
691 arising in a constant environment. BMC biology. 2021;19(1):1-21.

692 35. Lenski RE, Wiser MJ, Ribeck N, Blount ZD, Nahum JR, Morris JJ, et al. Sustained
693 fitness gains and variability in fitness trajectories in the long-term evolution experiment with
694 Escherichia coli. Proceedings of the Royal Society B: Biological Sciences.
695 2015;282(1821):20152292.

696 36. Wielgoss S, Barrick JE, Tenaillon O, Wiser MJ, Dittmar WJ, Cruveiller S, et al. Mutation
697 rate dynamics in a bacterial population reflect tension between adaptation and genetic load.
698 Proceedings of the National Academy of Sciences. 2013;110(1):222-7.

699 37. Rudan M, Schneider D, Warnecke T, Krisko A. RNA chaperones buffer deleterious
700 mutations in E. coli. Elife. 2015;4:e04745.

701 38. Bailey SF, Guo Q, Bataillon T. Identifying drivers of parallel evolution: A regression
702 model approach. Genome biology and evolution. 2018;10(10):2801-12.

703 39. Foster PL, Hanson AJ, Lee H, Popodi EM, Tang H. On the mutational topology of the
704 bacterial genome. G3: Genes, Genomes, Genetics. 2013;3(3):399-407.

705 40. Niccum BA, Lee H, MohammedIsmail W, Tang H, Foster PL. The Symmetrical Wave
706 Pattern of Base-Pair Substitution Rates across the Escherichia coli Chromosome Has Multiple
707 Causes. mBio. 2019;10(4).

708 41. Quandt EM, Gollihar J, Blount ZD, Ellington AD, Georgiou G, Barrick JE. Fine-tuning
709 citrate synthase flux potentiates and refines metabolic innovation in the Lenski evolution
710 experiment. Elife. 2015;4:e09696.

711 42. Zee PC, Mendes-Soares H, Yu YTN, Kraemer SA, Keller H, Ossowski S, et al. A shift
712 from magnitude to sign epistasis during adaptive evolution of a bacterial social trait. Evolution.
713 2014;68(9):2701-8.

714 43. Venkataram S, Monasky R, Sikaroodi SH, Kryazhimskiy S, Kacar B. Evolutionary
715 stalling and a limit on the power of natural selection to improve a cellular module. Proceedings
716 of the National Academy of Sciences. 2020;117(31):18582-90.

717 44. Rodrigues JV, Shakhnovich EI. Adaptation to mutational inactivation of an essential gene
718 converges to an accessible suboptimal fitness peak. Elife. 2019;8.

719 45. Kaznatcheev A. Computational complexity as an ultimate constraint on evolution.
720 Genetics. 2019;212(1):245-65.

721 46. Andersson DI, Slechta ES, Roth JR. Evidence that gene amplification underlies adaptive
722 mutability of the bacterial lac operon. Science. 1998;282(5391):1133-5.

723 47. Hendrickson H, Slechta ES, Bergthorsson U, Andersson DI, Roth JR. Amplification–
724 mutagenesis: evidence that "directed" adaptive mutation and general hypermutability result from
725 growth with a selected gene amplification. Proceedings of the National Academy of Sciences.
726 2002;99(4):2164-9.

727 48. Good BH, Desai MM. Evolution of mutation rates in rapidly adapting asexual
728 populations. Genetics. 2016;204(3):1249-66.

729 49. Philippe N, Crozat E, Lenski RE, Schneider D. Evolution of global regulatory networks
730 during a long-term experiment with Escherichia coli. Bioessays. 2007;29(9):846-60.

731 50. Chen H, Wu C-I, He X. The genotype–phenotype relationships in the light of natural
732 selection. Molecular biology and evolution. 2018;35(3):525-42.

733 51. Scott M, Gunderson CW, Mateescu EM, Zhang Z, Hwa T. Interdependence of cell
734 growth and gene expression: origins and consequences. Science. 2010;330(6007):1099-102.

735 52. Erickson DW, Schink SJ, Patsalo V, Williamson JR, Gerland U, Hwa T. A global
736 resource allocation strategy governs growth transition kinetics of Escherichia coli. Nature.
737 2017;551(7678):119-23.

738 53. Klumpp S, Hwa T. Bacterial growth: global effects on gene expression, growth feedback
739 and proteome partition. Current opinion in biotechnology. 2014;28:96-102.

740 54. Basan M, Hui S, Okano H, Zhang Z, Shen Y, Williamson JR, et al. Overflow metabolism
741 in Escherichia coli results from efficient proteome allocation. Nature. 2015;528(7580):99-104.

742 55. Mathis RA, Sokol ES, Gupta PB. Identification of Genes under Purifying Selection in
743 Human Cancers. BioRxiv. 2017:129205.

744 56. Weghorn D, Sunyaev S. Bayesian inference of negative and positive selection in human
745 cancers. Nature genetics. 2017;49(12):1785-8.

746 57. Patel SJ, Sanjana NE, Kishton RJ, Eidizadeh A, Vodnala SK, Cam M, et al. Identification
747 of essential genes for cancer immunotherapy. Nature. 2017;548(7669):537-42.

748 58. Li X, Giorgi EE, Marichannegowda MH, Foley B, Xiao C, Kong X-P, et al. Emergence
749 of SARS-CoV-2 through recombination and strong purifying selection. Science Advances.
750 2020;6(27):eabb9153.

751 59. Lieberman TD, Michel J-B, Aingaran M, Potter-Bynoe G, Roux D, Davis MR, et al.
752 Parallel bacterial evolution within multiple patients identifies candidate pathogenicity genes.
753 Nature genetics. 2011;43(12):1275-80.

754 60. Caballero JD, Clark ST, Coburn B, Zhang Y, Wang PW, Donaldson SL, et al. Selective
755 sweeps and parallel pathoadaptation drive Pseudomonas aeruginosa evolution in the cystic
756 fibrosis lung. MBio. 2015;6(5).

757 61. Chung H, Lieberman TD, Vargas SO, Flett KB, McAdam AJ, Priebe GP, et al. Global
758 and local selection acting on the pathogen Stenotrophomonas maltophilia in the human lung.
759 Nature communications. 2017;8:14078.

760 62. Cooper VS, Honsa E, Rowe H, Deitrick C, Iverson AR, Whittall JJ, et al. Experimental
761 Evolution in vivo to Identify Selective Pressures During Pneumococcal Colonization. Msystems.
762 2020;5(3).

763 63. Deatherage DE, Traverse CC, Wolf LN, Barrick JE. Detecting rare structural variation in
764 evolving microbial populations from new sequence junctions using breseq. Frontiers in genetics.
765 2015;5:468.

766 64. Haller BC, Messer PW. SLiM 3: forward genetic simulations beyond the Wright–Fisher
767 model. Molecular biology and evolution. 2019;36(3):632-7.

768 65. Robert L, Ollion J, Robert J, Song X, Matic I, Elez M. Mutation dynamics and fitness
769 effects followed in single cells. Science. 2018;359(6381):1283-6.

770 66. Perfeito L, Fernandes L, Mota C, Gordo I. Adaptive mutations in bacteria: high rate and
771 small effects. science. 2007;317(5839):813-5.
772

773

774 **FIGURES**
775
776 **Figure 1. Data analysis workflow.** 12 *E. coli* populations have evolved for more than 60,000
777 generations in Lenski's long-term evolution experiment (LTEE). We reanalyzed metagenomic
778 time series of the LTEE, described in Good et al. (2017). We also evolved 20 asexual haploid
779 populations *in silico* for 5,000 generations. We identified variants segregating during the
780 simulations to model metagenomic sequencing and variant calling. We designed a simple test to
781 infer mode of selection (STIMS) to test pre-defined query gene sets for positive or purifying
782 selection in the metagenomic time series. See the Materials and Methods for further details.

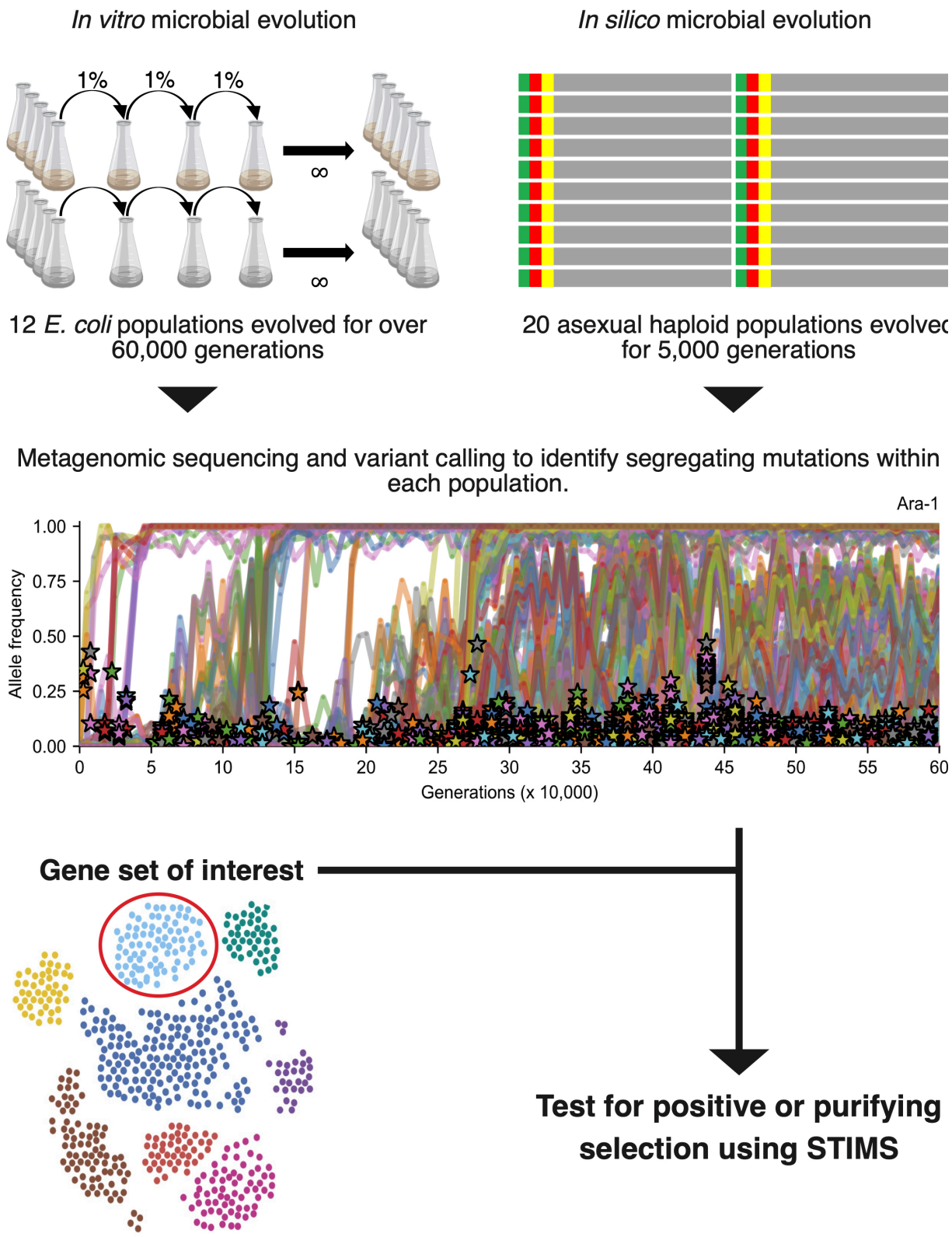
In vitro microbial evolution
In silico microbial evolution
1%
1%
1%
∞
∞
12 *E. coli* populations evolved for over 60,000 generations
20 asexual haploid populations evolved for 5,000 generations
Metagenomic sequencing and variant calling to identify segregating mutations within each population.
Ara-1
Allele frequency
1.00
0.75
0.50
0.25
0.00
0
5
10
15
20
25
30
35
40
45
50
55
60
Generations (x 10,000)
Gene set of interest
Test for positive or purifying selection using STIMS

785 **Figure 2. The STIMS algorithm.** When examining the evolutionary dynamics of a gene set of
786 interest, one often wants to know whether the set is enriched or depleted of observed mutations.
787 To test for depletion, we use the non-parametric bootstrap to estimate the fraction of randomized
788 gene sets that have fewer mutations than the query gene set. For example, if 11% of randomized
789 gene sets have fewer mutations than the query gene set, then the query gene set is not depleted of
790 mutations (one-tailed *p*-value = 0.11). A similar derivation holds for tests of enrichment. This
791 worked example uses the allele frequency dynamics of ribosome-associated proteins in the
792 Ara−1 population of Lenski's long term evolution experiment with *Escherichia coli* (LTEE) to
793 illustrate how the STIMS algorithm works. This population evolved a hypermutator phenotype
794 around the 26,250-generation time point.
795

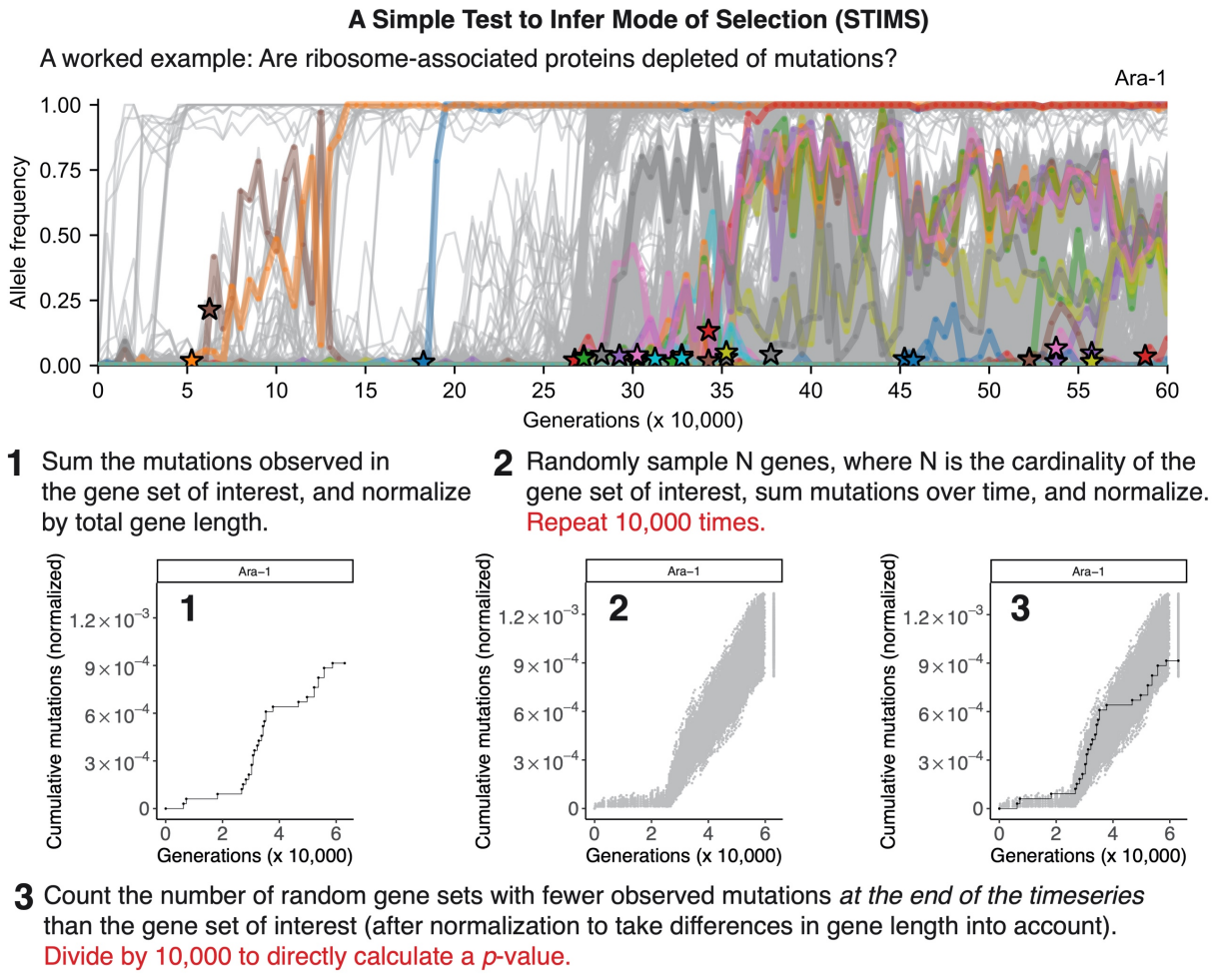

796

797 **Figure 3. *In silico* evolution experiments demonstrate that STIMS can detect positive but**
798 **not purifying selection in nonmutator populations.** Bacterial evolution was simulated using a
799 Wright-Fisher model. Each simulation lasted 5,000 generations. The effective population size
800 was set to 1 million individuals. Nonmutator bacteria were modeled using a mutation rate of
801 10^{-10} per base-pair per generation. Each individual contains an idealized genome of 4,000 genes,
802 each 1,000 base-pairs in length, for a genome of 4 million base-pairs. 100 genes are targets of
803 positive selection, 100 genes are evolving completely neutrally (relaxed selection), and 100
804 genes are evolving under purifying selection. The remaining 3,700 genes evolve nearly neutrally,
805 based on published estimates of the genomic distribution of mutation fitness effects in
806 *Escherichia coli*. See the Materials and Methods for further details. A) Typical allele frequency
807 dynamics of a nonmutator population, showing selective sweeps and clonal interference. B)
808 STIMS shows high sensitivity and specificity for detecting positive selection in nonmutator
809 populations. C) STIMS is unable to detect purifying selection (low sensitivity), but shows no
810 false positives (high specificity). D) Typical result of running STIMS on genes evolving under
811 positive selection in the nonmutator simulations. E) Typical result of running STIMS on genes
812 evolving neutrally in the nonmutator simulations. F) Typical result of running STIMS on genes
813 evolving under purifying selection in the nonmutator simulations.
814

Nonmutator: N_e = 1,000,000 individuals and $\mu = 10^{-10}$ (bp^{-1} $generation^{-1}$)

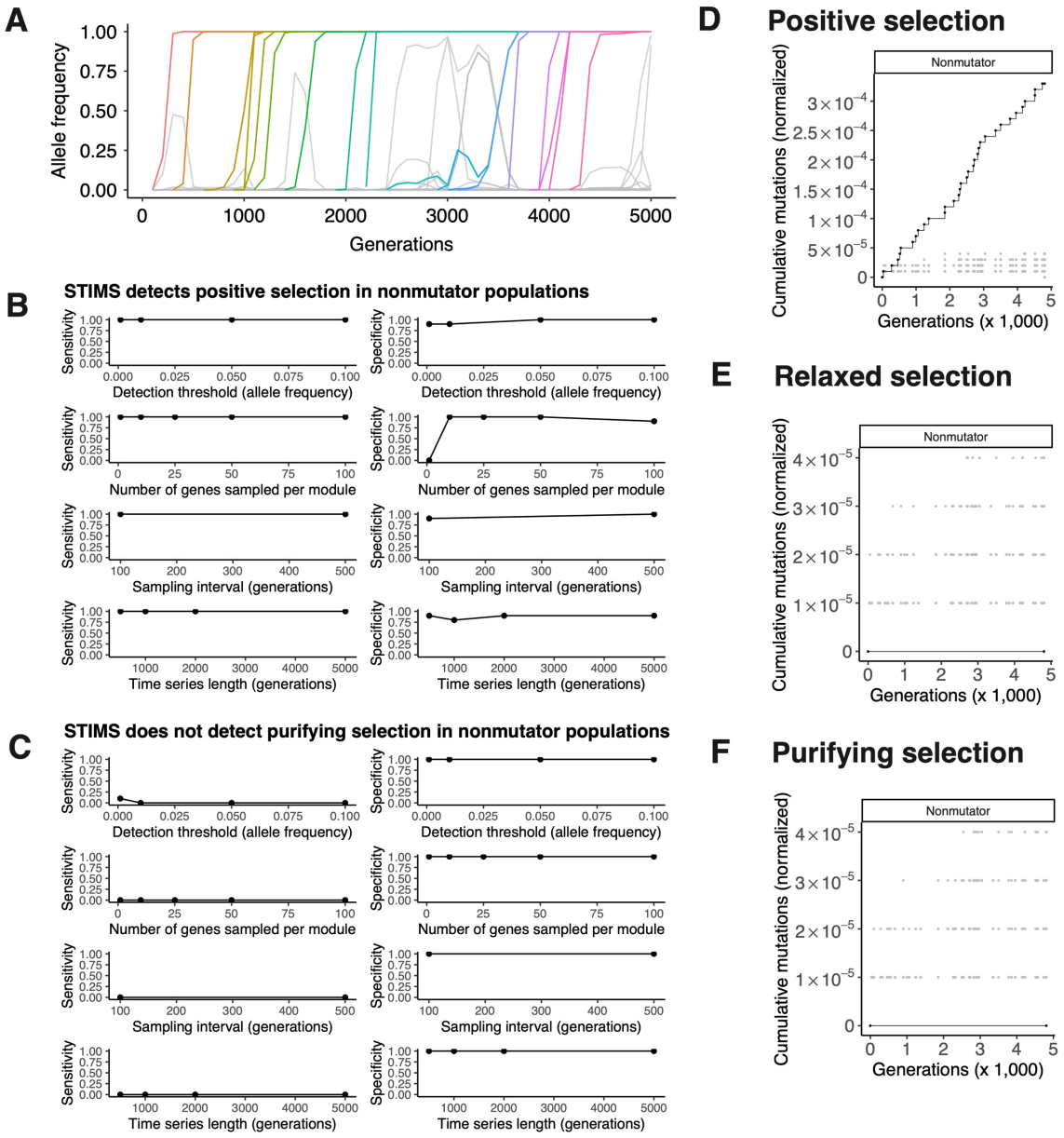

817 **Figure 4. *In silico* evolution experiments demonstrate that STIMS can detect both positive**
818 **and purifying selection in hypermutator populations.** Bacterial evolution was simulated using
819 a Wright-Fisher model. Each simulation lasted 5,000 generations. The effective population size
820 was set to 1 million individuals. Hypermutator bacteria were modeled using a mutation rate of
821 10^{-8} per base-pair per generation. Each individual contains an idealized genome of 4,000 genes,
822 each 1,000 base-pairs in length, for a genome of 4 million base-pairs. 100 genes are targets of
823 positive selection, 100 genes are evolving completely neutrally (relaxed selection), and 100
824 genes are evolving under purifying selection. The remaining 3,700 genes evolve nearly neutrally,
825 based on published estimates of the genomic distribution of mutation fitness effects in
826 *Escherichia coli*. See the Materials and Methods for further details. A) Typical allele frequency
827 dynamics of a hypermutator population, showing selective sweeps and clonal interference. B)
828 STIMS shows high sensitivity and specificity for detecting positive selection in hypermutator
829 populations. C) STIMS detects purifying selection with increasing sensitivity at lower allele
830 frequency mutation detection thresholds, more genes sampled from the set of genes evolving
831 under purifying selection, the length of the time series, and shorter intervals between
832 metagenomic sampling, and shows high specificity across all tested parameters. D) Typical result
833 of running STIMS on genes evolving under positive selection in the hypermutator simulations.
834 E) Typical result of running STIMS on genes evolving neutrally in the hypermutator simulations.
835 F) Typical result of running STIMS on genes evolving under purifying selection in the
836 hypermutator simulations.
837

Hypermutator: N_e = 1,000,000 individuals and $\mu = 10^{-8}$ (bp^{-1} $generation^{-1}$)

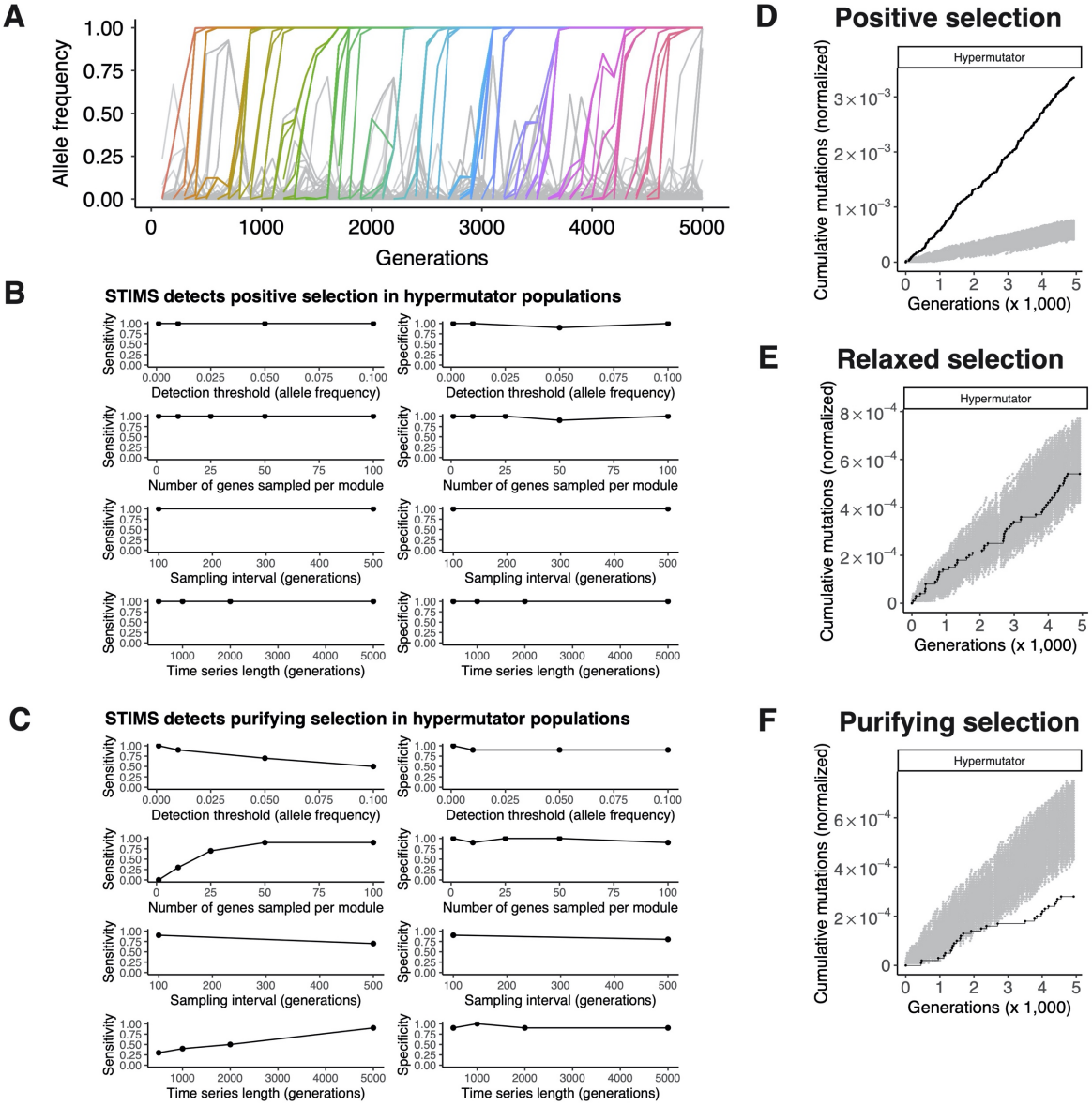

840 **Figure 5. Gold-standard genes under relaxed selection.** Each panel shows the cumulative
841 number of mutations in the gold-standard neutral genes (black) in the 12 LTEE populations. For
842 comparison, random sets of 57 genes were sampled 1,000 times, and the cumulative number of
843 mutations in those random gene sets, normalized by gene length, were calculated. The middle
844 95% of this null distribution is shown in gray, in order to show a two-tailed statistical
845 comparison of the cumulative number of mutations in the gold-standard neutral gene set to the
846 null distribution at $\alpha = 0.05$. The top six panels are populations with the ancestral mutation rate
847 (nonmutator populations) and the bottom six panels are those that evolved elevated mutation
848 rates (hypermutator populations).
849

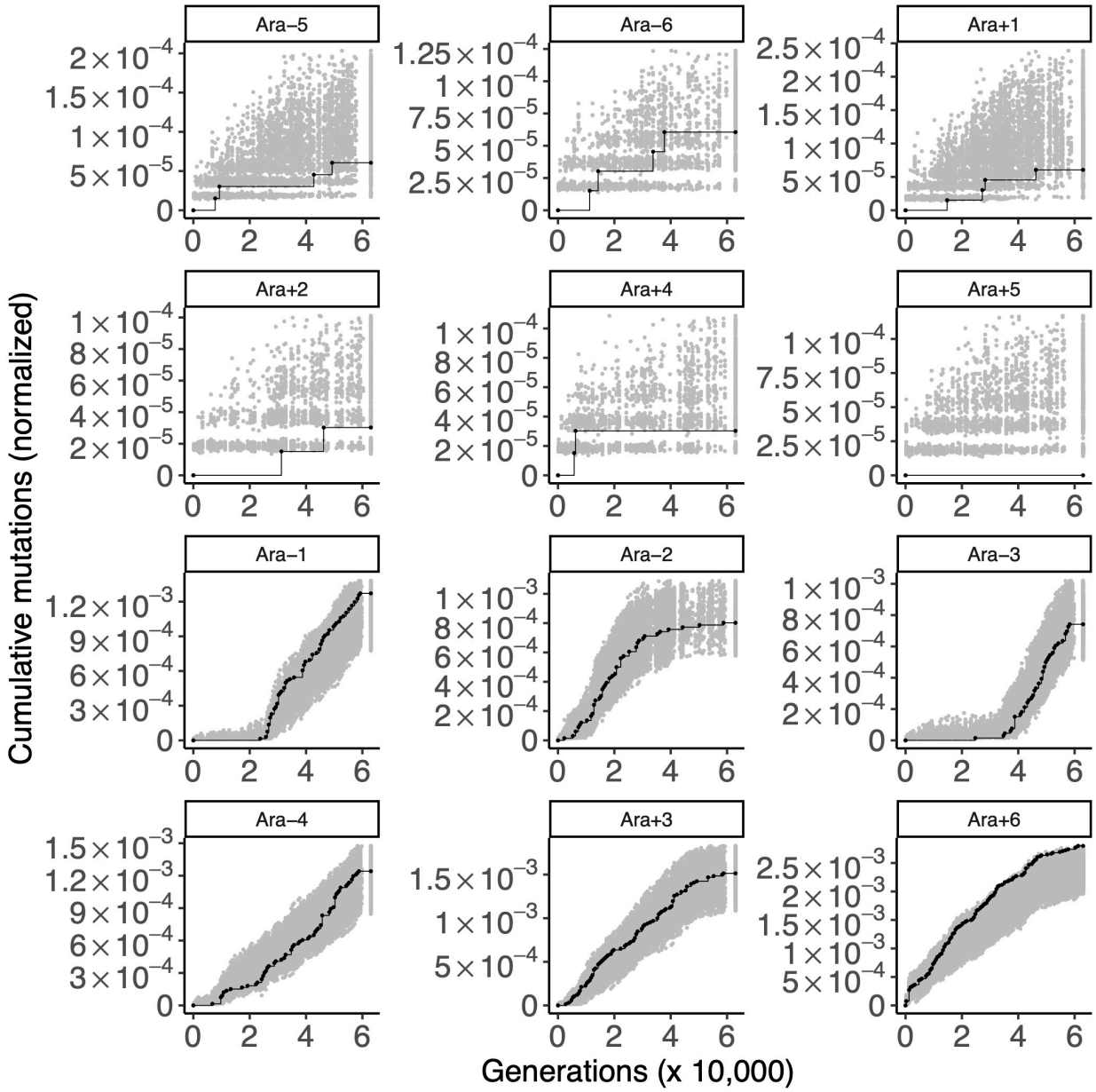

850
851
852

853 **Figure 6. Gold-standard genes under purifying selection.** Each panel shows the cumulative
854 number of mutations in the gold standard set of genes under purifying selection (black) in the 12
855 LTEE populations. For comparison, random sets of 490 genes were sampled 1,000 times, and the
856 cumulative number of mutations in those random gene sets, normalized by gene length, were
857 calculated. The middle 95% of this null distribution is shown in gray. The top six panels are the
858 nonmutator populations and the bottom six panels are the hypermutator populations.
859

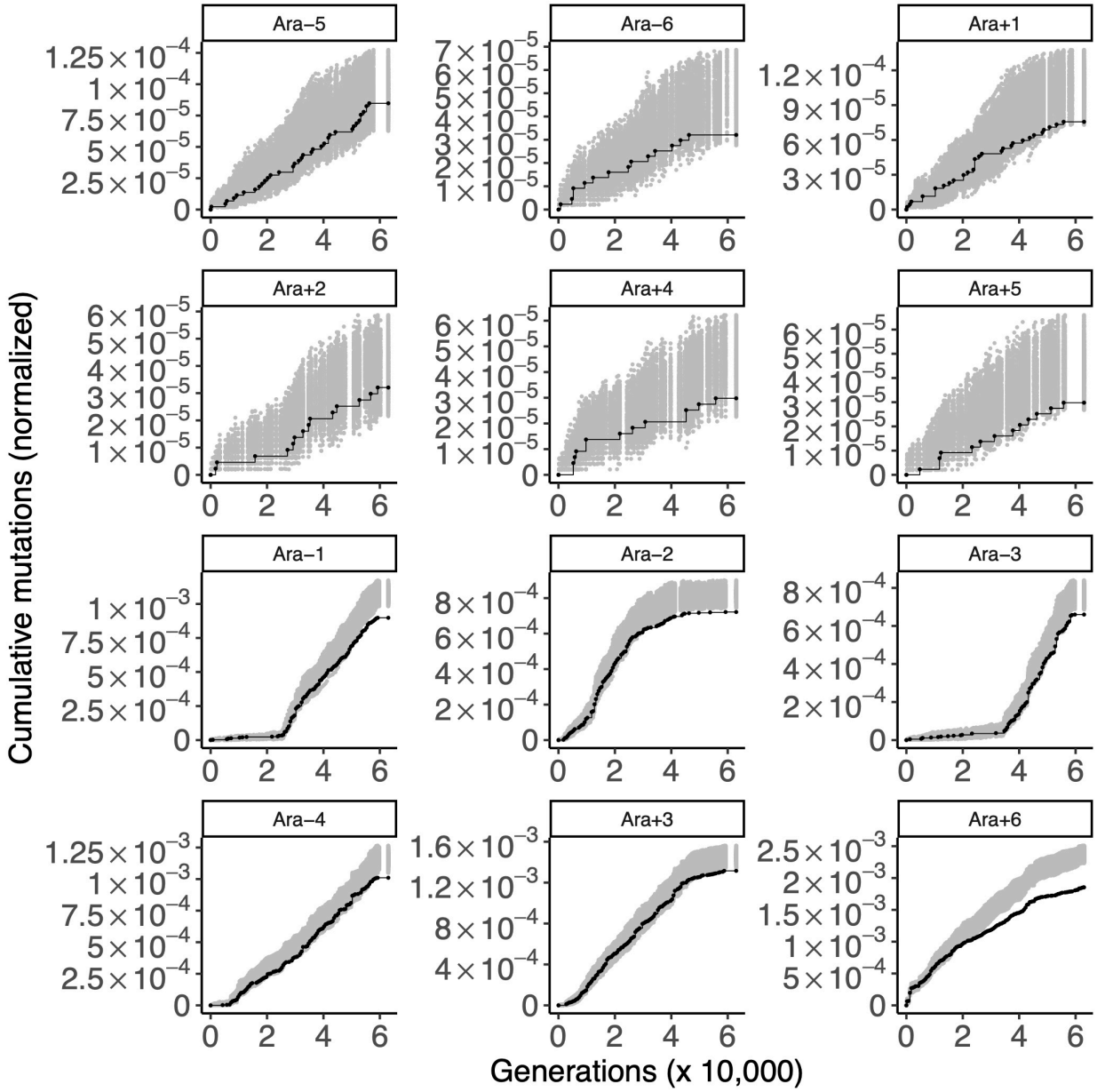

860
861
862
863
864

Figure 7. Gold-standard genes under positive selection. Each panel shows the cumulative number of mutations in the gold standard set of genes under positive selection (black) in the 12 LTEE populations. These genes are the 50 genes with the strongest signal of parallel evolution in clones isolated from the six nonmutator populations, as scored by Tenaillon et al. (2016). For comparison, random sets of 50 genes were sampled 1,000 times, and the cumulative number of mutations in those random gene sets, normalized by gene length, were calculated. The middle 95% of this null distribution is shown in gray. The top six panels are the nonmutator populations and the bottom six panels are the hypermutator populations.

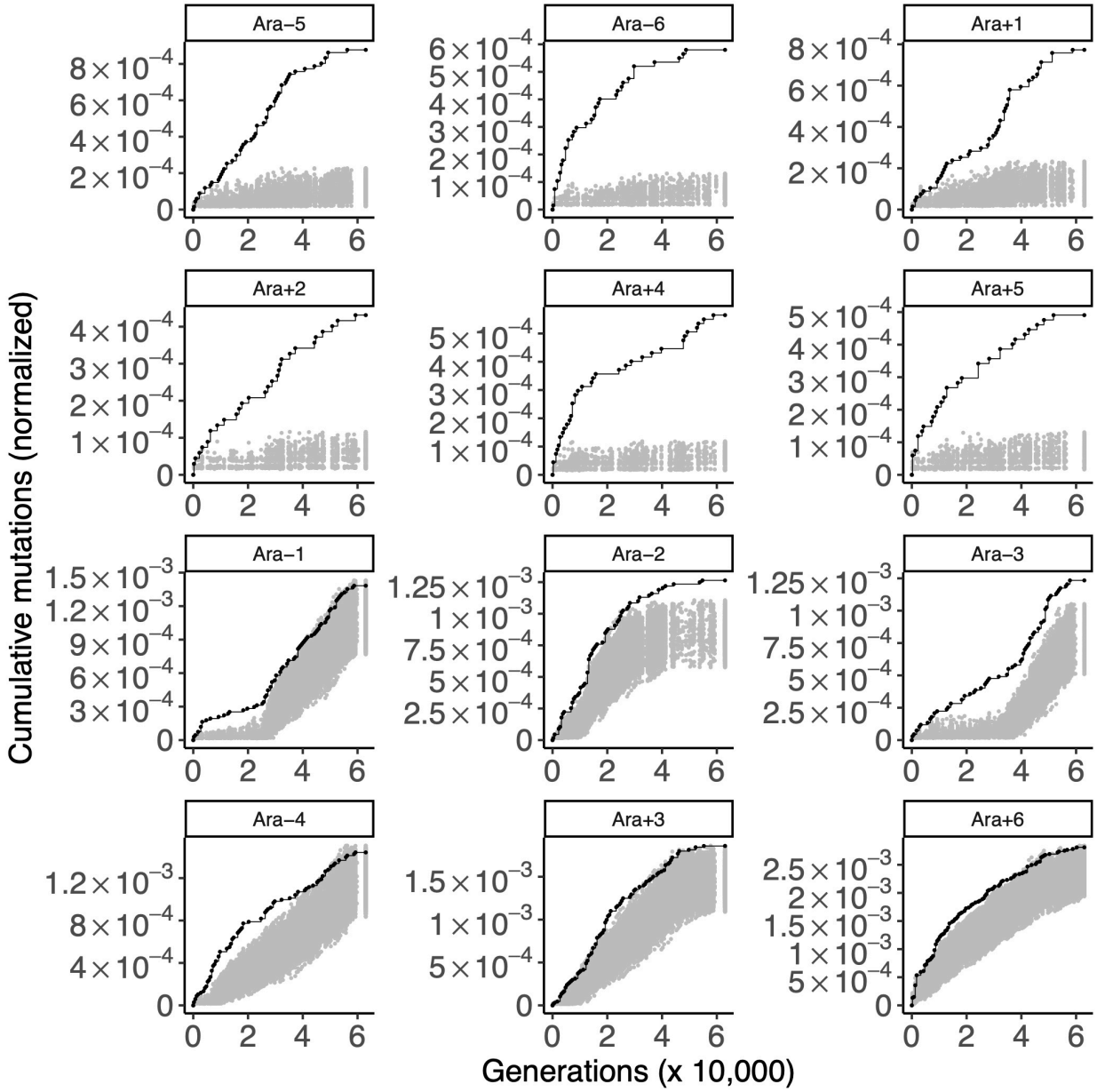

Figure 8. I-modulon regulators evolve under strong positive selection, while genes regulated within I-modulon evolve under weaker selection. Each panel shows the cumulative number of mutations in 70 I-modulon regulators (black) and in 1,394 genes regulated within I-modulons (red) in the 12 LTEE populations. For comparison to the I-modulon regulators, random sets of 70 genes were sampled 1,000 times, and the cumulative number of mutations in those random gene sets, normalized by gene length, were calculated. The middle 95% of the null distribution for I-modulon regulators is shown in gray. A similar procedure was used with random sets of 1,394 genes to make a null distribution in pink to compare to the genes regulated within I-modulons. The top six panels are the nonmutator populations and the bottom six panels are the hypermutator populations.

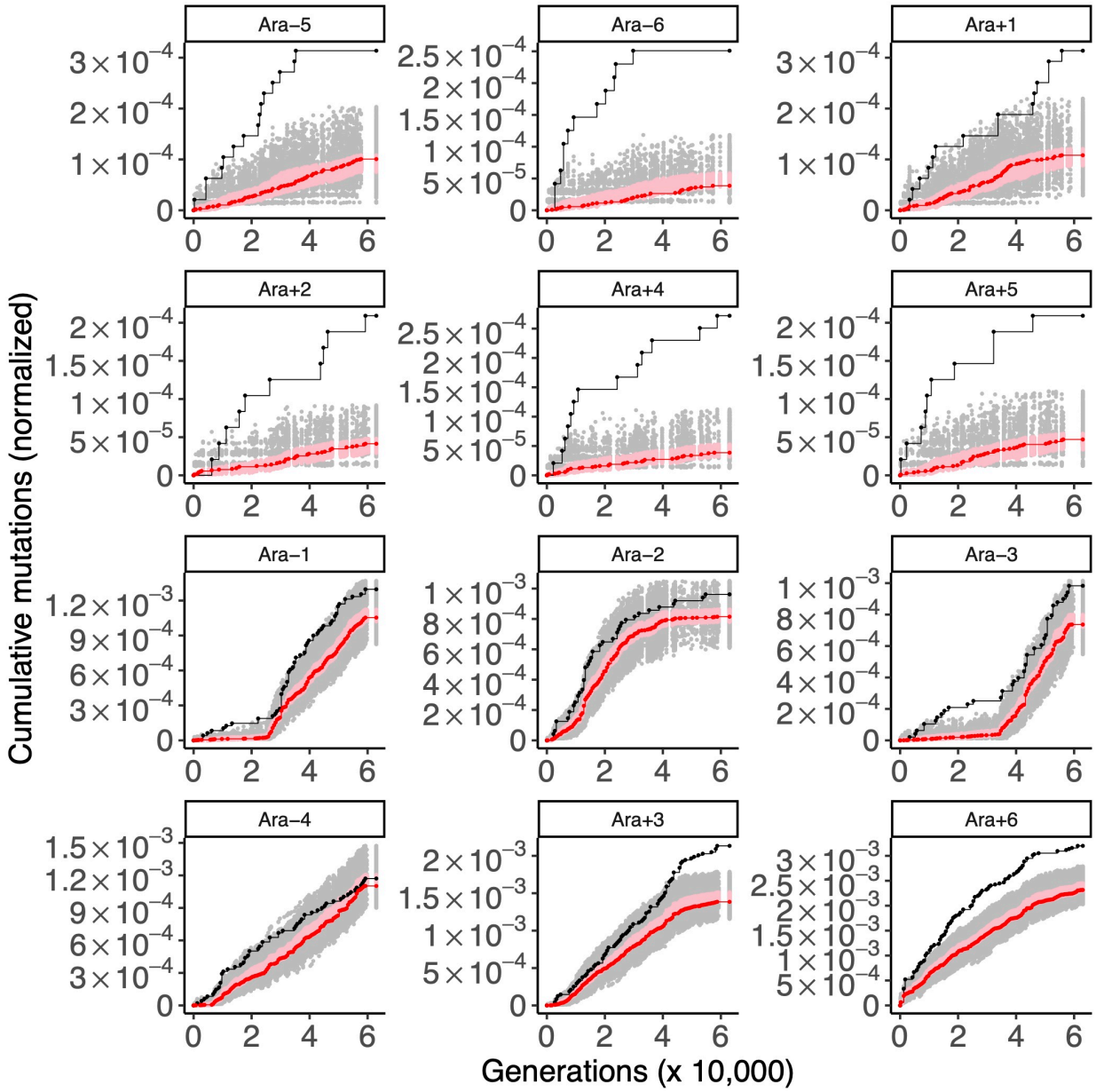

Figure 9. Regulatory genes are under positive selection in hypermutator *Pseudomonas aeruginosa* populations evolving under subinhibitory concentrations of colistin. The cumulative number of mutations in 424 annotated regulatory genes in two replicate populations of hypermutator *P. aeruginosa* is shown in black. For comparison, random sets of 424 genes were sampled 1,000 times, and the cumulative number of mutations in those random gene sets, normalized by gene length, were calculated. The middle 95% of this null distribution is shown in gray.

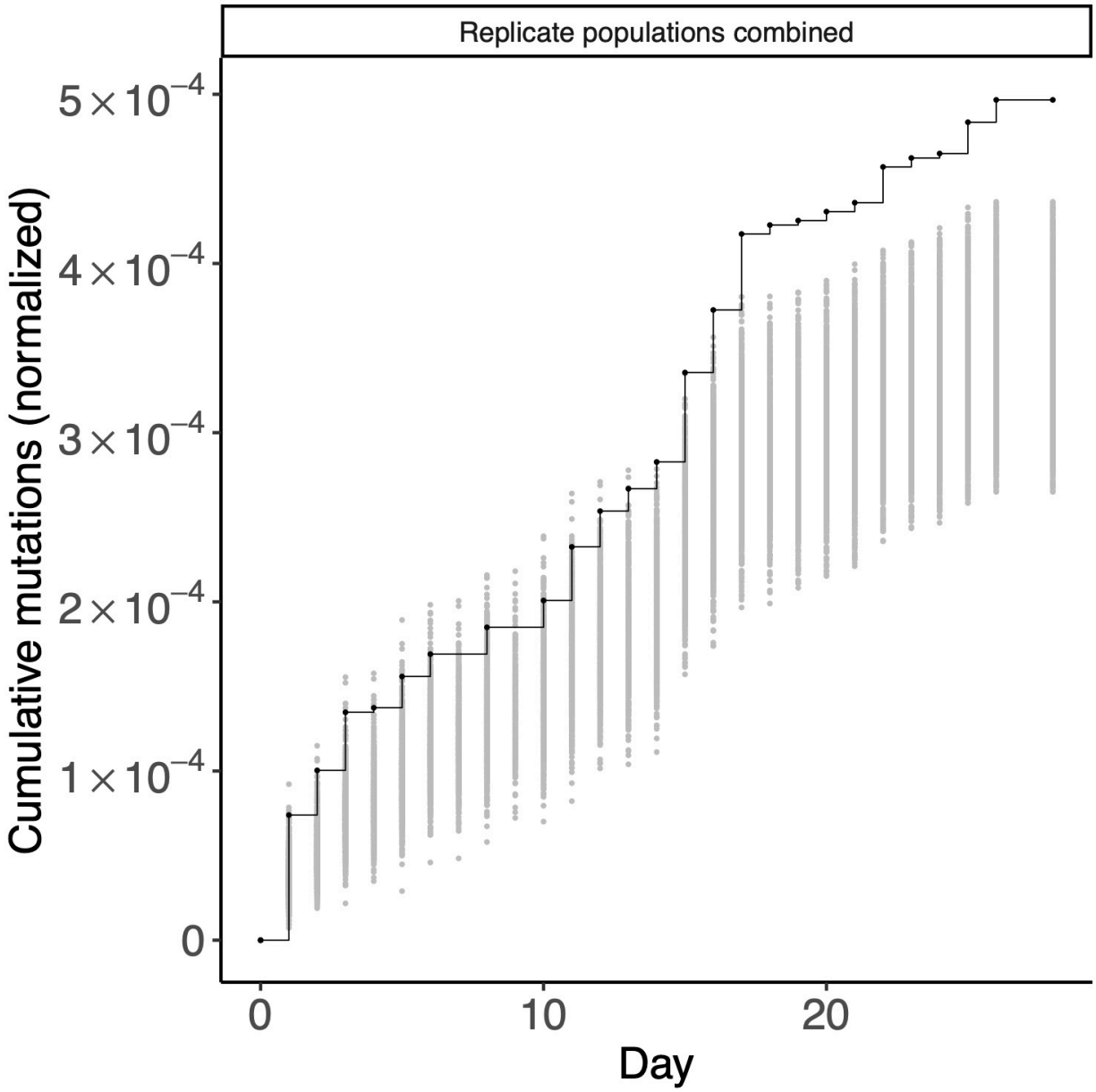

SUPPLEMENTARY INFORMATION:

Supplementary File 1. Results of running STIMS, over all LTEE populations, on each I-modulon in Sastry et al. (2019).

Supplementary File 2. Results of running STIMS, individually on each each LTEE population, on each I-modulon in Sastry et al. (2019).

Supplementary File 3. Results of running Poisson method as a genome-wide screen for positive and purifying selection, over all LTEE populations, and individually on each LTEE population.

917 **SUPPLEMENTARY TEXT**

918

919 *Comparison of STIMS to a test for selection based on the Poisson distribution*

920 One class of statistical tests for selection in evolution experiments uses the Poisson
921 distribution to model the expected distribution of mutations per genomic site per unit time under
922 neutral evolution [16, 34]. Using this framework, significant deviations from the Poisson null
923 expectation can indicate positive or purifying selection. In principle, Poisson methods should be
924 simpler to implement and computationally cheaper than STIMS. However, methods based on the
925 Poisson distribution may be sensitive to model misspecification, due to local mutation biases that
926 can cause deviation from the Poisson expectation in the absence of selection [31]. Variations of
927 the bootstrapping approach used by STIMS, on the other hand, can account for such mutational
928 biases through randomization (Materials and Methods).

929 To better understand the relative strengths and weaknesses of STIMS in comparison to
930 Poisson methods, we implemented the Poisson method used by Kinnersley *et al.* [34], and re-ran
931 all of our positive control experiments on gold-standard sets of genes (Materials and Methods).
932 Overall, both STIMS and the Poisson method give similar results. The Poisson method
933 successfully recovers signals of purifying selection ($p < 10^{-14}$) and positive selection ($p < 10^{-50}$)
934 on the respective sets of gold-standard genes. However, the Poisson method finds a weak signal
935 of positive selection on the gold-standard set of genes under relaxed selection ($p = 0.0397$). The
936 Poisson method finds a signal of purifying selection on most proteome sectors (FDR-corrected p
937 $< 10^{-11}$ for U-sector; FDR-corrected $p < 0.00001$ for A-sector; FDR-corrected $p = 0.000162$ for
938 R-sector; FDR-corrected $p = 0.00182$ for S-sector; FDR-corrected $p = 0.00217$ for O-sector;
939 FDR-corrected $p = 0.391$ for C-sector). Eigengenes show little to no evidence of selection under
940 the Poisson method (FDR-corrected $p = 0.0327$ for Eigengene 2; the rest are nonsignificant). I-
941 modulon regulators show evidence of very strong positive selection ($p < 10^{-13}$), while 16 I-
942 modulons show evidence of either positive or purifying selection at a Benjamini-Hochberg
943 corrected p-value threshold of 0.01 (Supplementary Table 4). 14 out of these 16 I-modulons are
944 significant by STIMS, while the other two, "flu-yeeRS" and "Pyruvate", trend toward
945 significance (Supplementary File S1). Finally, we used the Poisson method as a genome-wide
946 screen for positive and purifying selection, both over all LTEE populations, and on each
947 population individually. We report these results at a Benjamini-Hochberg corrected p-value

948 threshold of 0.01 in Supplementary File S3. Most of the genes showing evidence of positive
949 selection have been reported before [15, 16, 23]. However, this screen finds 7 genes with a
950 significant signal of purifying selection across the LTEE, none of which have been reported
951 before: *acnB* (aconitate hydratase), *ybjL* (hypothetical protein), *yhdP* (conserved membrane
952 protein predicted transporter), *recG* (ATP-dependent DNA helicase), *cyoB* (cytochrome o
953 ubiquinol oxidase subunit I), *wcaJ* (predicted UDP-glucose lipid carrier transferase), and *atpD*
954 (F0F1 ATP synthase subunit beta). All of these genes are longer than 1,300 bp, and three of them
955 (*ybjL*, *wcaJ*, and *atpD*) have no observed mutations at all.
956 Altogether, this detailed comparison indicates the Poisson method is faster and is more
957 practical for genome-wide scans for positive and purifying selection on single genes, but that its
958 sensitivity comes at the price of more false positives. STIMS is more conservative than the
959 Poisson method, and gives results that are more consistent with ground truth, as defined by the
960 sets of gold-standard genes that we used for empirical validation. STIMS, unlike the Poisson
961 method, also provides a picture of the tempo of evolution in a gene set over time, as well as
962 changes in statistical significance over time. These visualizations are especially useful for
963 observing *how* the tempo of evolutionary change in a gene set of interest changes over time, and
964 for generating further hypotheses and predictions for empirical validation (Supplementary Files 1
965 and 2).
966
967

968 **SUPPLEMENTARY TABLES AND FIGURES**
969
970 **Supplementary Table S1. Essential genes in REL606 with no observed mutations in the**
971 **LTEE metagenomics data.**
972

Gene	Locus tag	Gene length	Product
rlpB	ECB_00610	582	minor lipoprotein
rplJ	ECB_03861	498	50S ribosomal protein L10
ECB_01539	ECB_01539	408	protein similar to DicA regulator of DicB encoded by prophage CP-933O
sdhD	ECB_00682	348	succinate dehydrogenase cytochrome b556 small membrane subunit
rplV	ECB_03166	333	50S ribosomal protein L22
rpsJ	ECB_03172	312	30S ribosomal protein S10
rpsN	ECB_03158	306	30S ribosomal protein S14
yrbB	ECB_03056	294	hypothetical protein
groES	ECB_04012	294	co-chaperonin GroES
rpsS	ECB_03167	279	30S ribosomal protein S19
rpsT	ECB_00027	264	30S ribosomal protein S20
rpsQ	ECB_03162	255	30S ribosomal protein S17
atpE	ECB_03621	240	F0F1 ATP synthase subunit C
rpmC	ECB_03163	192	50S ribosomal protein L29
ydaE	ECB_01329	171	conserved protein
rpmJ	ECB_03150	117	50S ribosomal protein L36
ybgT	ECB_00694	114	hypothetical protein
rhoL	ECB_03660	102	rho operon leader peptide

973
974

975
976 **Supplementary Table S2. Essential genes in REL606 with only synonymous mutations in**
977 **the LTEE metagenomics data.**
978

Gene	Locus tag	Gene length	Product
atpD	ECB_03616	1383	F0F1 ATP synthase subunit beta
icdA	ECB_01134	1251	isocitrate dehydrogenase
thyA	ECB_02675	795	thymidylate synthase
plsC	ECB_02890	738	1-acyl-sn-glycerol-3-phosphate acyltransferase
pdxH	ECB_01608	657	pyridoxamine 5'-phosphate oxidase
rplD	ECB_03170	606	50S ribosomal protein L4
lpcA	ECB_00217	579	phosphoheptose isomerase
rimM	ECB_02497	549	16S rRNA-processing protein
rplE	ECB_03159	540	50S ribosomal protein L5
sixA	ECB_02264	486	phosphohistidine phosphatase
folK	ECB_00141	480	2-amino-4-hydroxy-6-hydroxymethyldihyropteridine pyrophosphokinase
accB	ECB_03113	471	acetyl-CoA carboxylase
holD	ECB_04247	414	DNA polymerase III subunit psi
rpsI	ECB_03090	393	30S ribosomal protein S9
iscU	ECB_02421	387	scaffold protein
rplQ	ECB_03145	384	50S ribosomal protein L17
panD	ECB_00130	381	aspartate 1-decarboxylase precursor
rpsL	ECB_03193	375	30S ribosomal protein S12
rplN	ECB_03161	372	50S ribosomal protein L14
rnpA	ECB_03587	360	ribonuclease P
rplT	ECB_01685	357	50S ribosomal protein L20
yadR	ECB_00155	345	hypothetical protein
fdx	ECB_02417	336	[2Fe-2S] ferredoxin
secG	ECB_03040	333	protein-export membrane protein
ybaB	ECB_00422	330	hypothetical protein
acpP	ECB_01090	237	acyl carrier protein
rpmI	ECB_01686	198	50S ribosomal protein L35
rpmH	ECB_03586	141	50S ribosomal protein L34
pheL	ECB_02487	48	pheA gene leader peptide
trpL	ECB_01239	45	trp operon leader peptide

979
980

981 **Supplementary Table S3. I-modulons showing evidence of selection, historical contingency**
982 **and epistasis in the LTEE, using STIMS.**
983

Page*	I-modulon	Populations of Interest	Hypothesis
3	ArcA-2	Ara−2, Ara−3	purifying selection
11	CpxR	Ara−3, Ara−4, Ara+6	positive and purifying selection
13	Crp-1	Ara−5, Ara+1	positive selection
16	CsqR	Ara+3, Ara+6	purifying selection
18	CysB	Ara−1, Ara+6	purifying selection
19	Deletion-1	Ara−3	positive selection
22	Duplication-1	Ara−2, Ara−3, Ara−4, Ara+3	strong purifying selection
23	e14-deletion	Ara−3	strong positive selection
24	efeU-repair	Ara+3, Ara+6	strong positive selection, purifying selection
28	FadR	Ara−1, Ara−2, Ara+6	purifying selection
30	fimbriae	Ara−2	strong positive selection
31	FlhDC	Ara−2, Ara+6	positive selection
37	fur-KO	Ara−3	strong positive selection
38	GadEWX	Ara−1, Ara−3, Ara+6	positive selection
40	GadWX-KO	Ara+6	positive selection
46	insertion	Ara−1, Ara+6	strong positive selection
48	Leu/Ile	Ara−1, Ara−4, Ara+3, Ara+6	strong purifying selection
49	lipopolysaccharide	Ara−1	strong positive selection
50	Lrp	Ara+6	purifying selection
53	MetJ	Ara−4, Ara+3, Ara+6	purifying selection
63	PurR-1	Ara−1	purifying selection
69	RcsAB	Ara−3, Ara+3	purifying selection
72	sgrT	Ara−1, Ara−4,	purifying selection
77	translation	Ara+1, Ara+2, Ara+5, Ara−3, Ara+6	positive and purifying selection
79	uncharacterized-1	Ara+2, Ara+5, Ara+3	positive selection
81	uncharacterized-3	Ara−1	positive selection
82	uncharacterized-4	Ara−6, Ara+1, Ara+2, Ara+4, Ara+5, Ara−2, Ara−3, Ara−4, Ara+3, Ara+6	strong positive and purifying selection
90	YieP	Ara−2, Ara−4	positive selection

984 *Page numbers refers to Supplementary Files 1 (STIMS across all LTEE populations) and
985 Supplementary File 2 (STIMS on individual LTEE populations).

986 **Supplementary Table S4. I-modulons showing evidence of selection across all LTEE**
987 **populations based on the Poisson method, at a FDR-corrected *p*-value threshold of 0.01.**
988

I-modulon	FDR-corrected *p*-value	Inference
CysB	$p < 10^{-5}$	purifying selection
Leu/Ile	$p < 10^{-5}$	purifying selection
Duplication-1	$p < 10^{-4}$	purifying selection
fimbrae	$p < 10^{-4}$	purifying selection
RcsAB	$p = 0.000172$	purifying selection
Crp-1	$p = 0.000317$	positive selection
flu-yeeRS	$p = 0.000636$	positive selection
MetJ	$p = 0.000877$	purifying selection
FadR	$p = 0.000989$	purifying selection
Pyruvate	$p = 0.00241$	purifying selection
translation	$p = 0.00268$	purifying selection
CsqR	$p = 0.00288$	purifying selection
Lrp	$p = 0.00347$	purifying selection
ArcA-2	$p = 0.00358$	purifying selection
GadEWX	$p = 0.00369$	positive selection
Insertion	$p = 0.00775$	positive selection

989

Supplementary Figure S1. Gold-standard genes under relaxed selection. Each panel shows the cumulative number of mutations in the gold-standard neutral genes (black) in all 12 LTEE populations. For comparison, random sets of 57 genes were sampled 1,000 times, and the cumulative number of mutations in those random gene sets, normalized by gene length, were calculated. The middle 95% of this null distribution is shown in gray, in order to show a two-tailed statistical comparison of the cumulative number of mutations in the gold-standard neutral gene set to the null distribution at $\alpha = 0.05$.

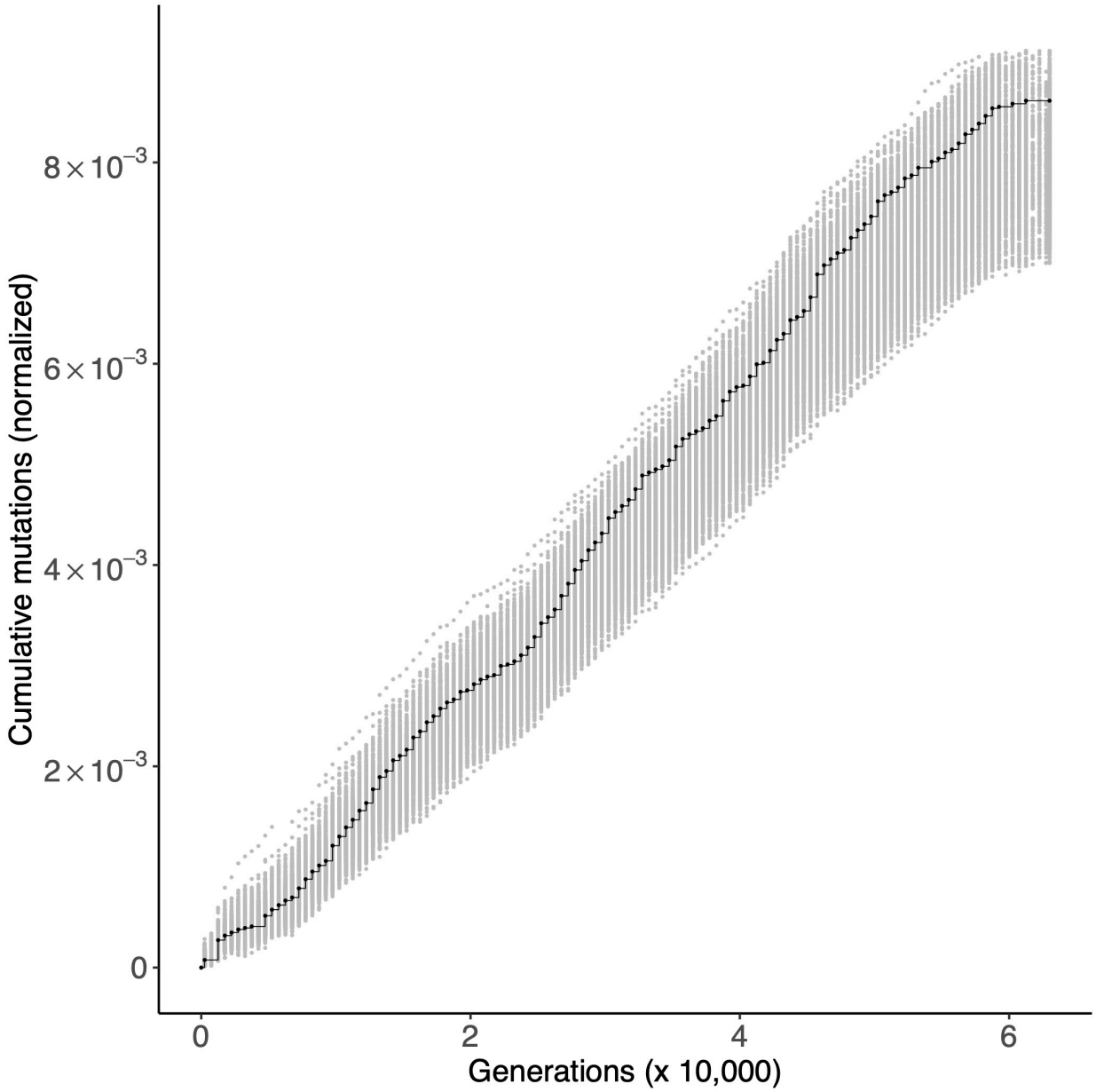

1001 **Supplementary Figure S2. Gold-standard genes under purifying selection.** Each panel shows
1002 the cumulative number of mutations in the gold standard set of genes under purifying selection
1003 (black) in all 12 LTEE populations. For comparison, random sets of 490 genes were sampled
1004 1,000 times, and the cumulative number of mutations in those random gene sets, normalized by
1005 gene length, were calculated. The middle 95% of this null distribution is shown in gray.

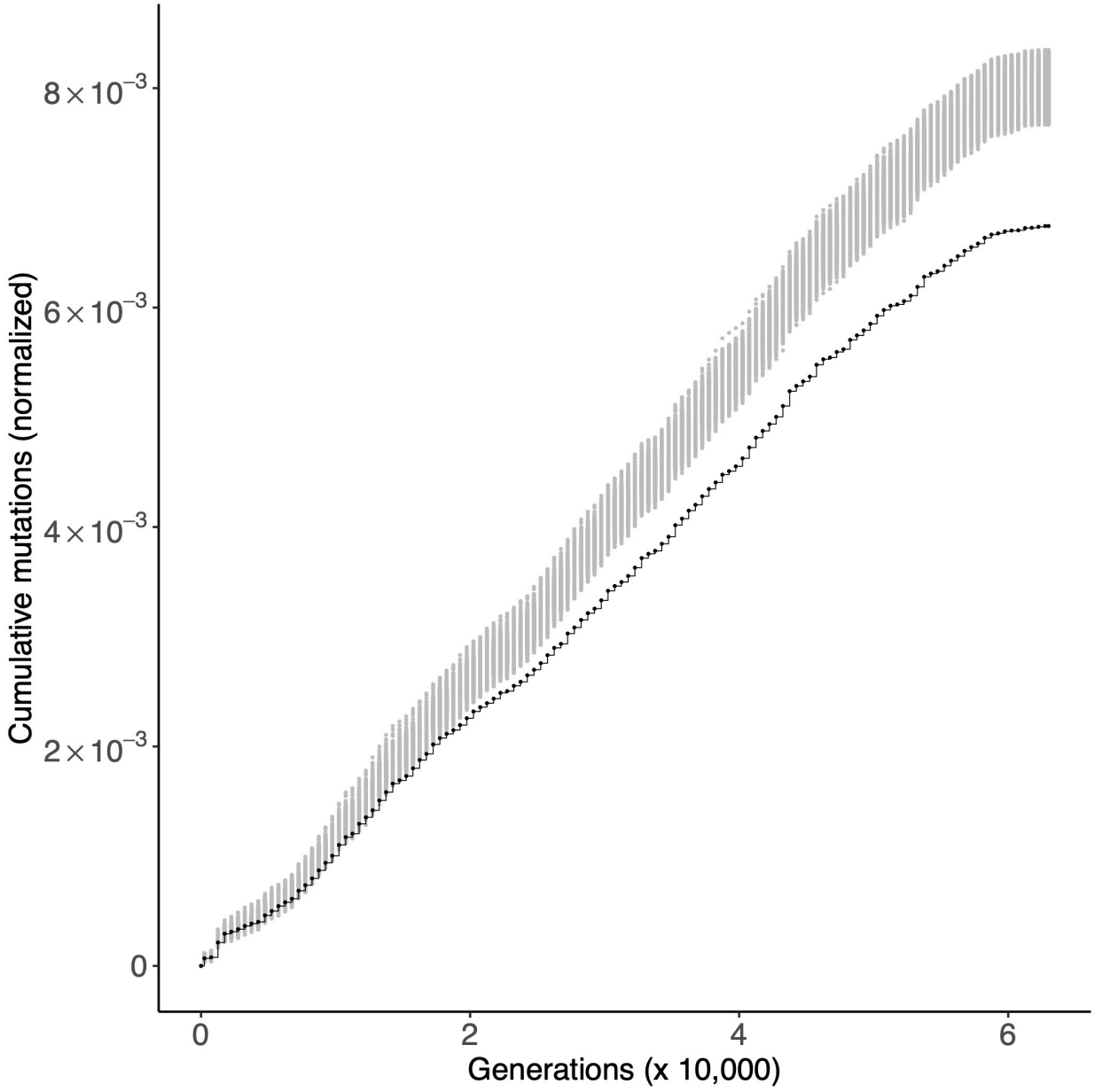

1006

1007 **Supplementary Figure S3. Gold-standard genes under positive selection.** Each panel shows
1008 the cumulative number of mutations in the gold standard set of genes under positive selection
1009 (black) in all 12 LTEE populations. These genes are the 50 genes with the strongest signal of
1010 parallel evolution in clones isolated from the six nonmutator populations, as scored by Tenaillon
1011 et al. (2016). For comparison, random sets of 50 genes were sampled 1,000 times, and the
1012 cumulative number of mutations in those random gene sets, normalized by gene length, were
1013 calculated. The middle 95% of this null distribution is shown in gray.

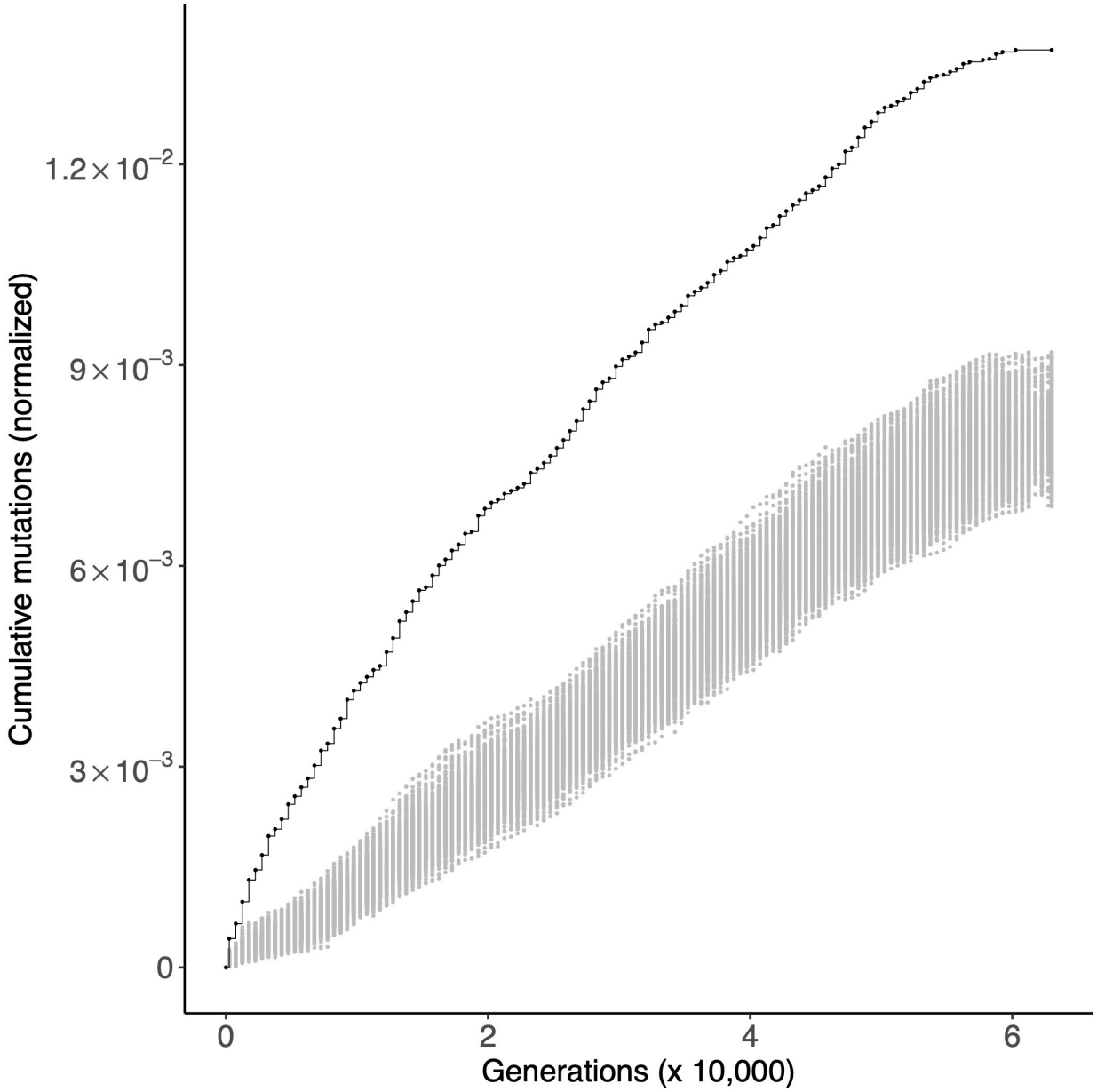

1014

Supplementary Figure S4. Genes evolving in parallel in hypermutator populations. Each panel shows the cumulative number of mutations in the 50 genes with the strongest signal of parallel evolution in clones isolated from the six hypermutator populations, as scored by Tenaillon et al. (2016), in the 12 LTEE populations. These curves are drawn in black. For comparison, random sets of 50 genes were sampled 1,000 times, and the cumulative number of mutations in those random gene sets, normalized by gene length, were calculated. The middle 95% of this null distribution is shown in gray. The top six panels are the nonmutator populations and the bottom six panels are the hypermutator populations.

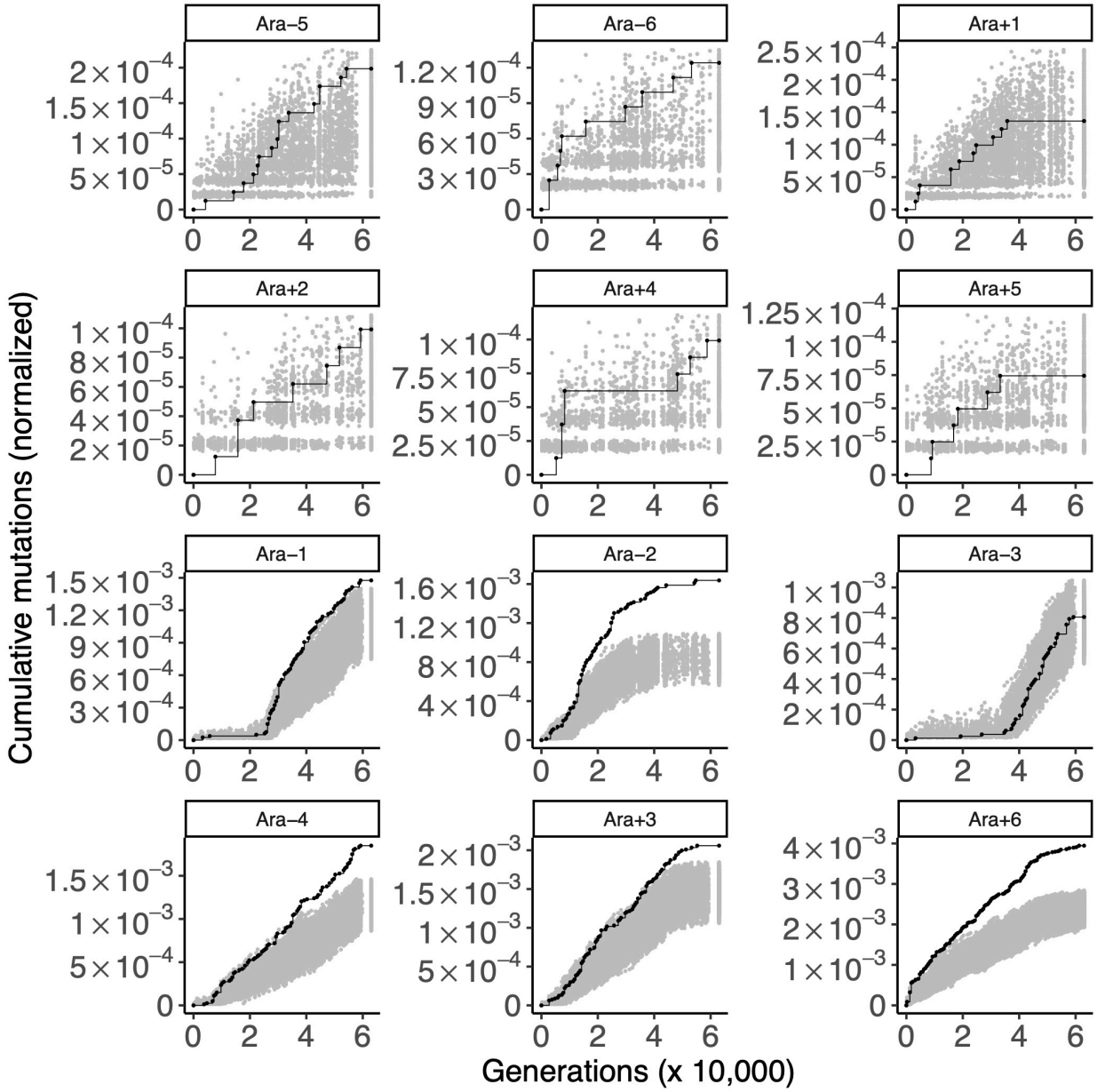

1027 **Supplementary Figure S5. Genes evolving in parallel in hypermutator populations.** Each
1028 panel shows the cumulative number of mutations in the 50 genes with the strongest signal of
1029 parallel evolution in clones isolated from the six hypermutator populations, as scored by
1030 Tenaillon et al. (2016), in all 12 LTEE populations. These curves are drawn in black. For
1031 comparison, random sets of 50 genes were sampled 1,000 times, and the cumulative number of
1032 mutations in those random gene sets, normalized by gene length, were calculated. The middle
1033 95% of this null distribution is shown in gray.

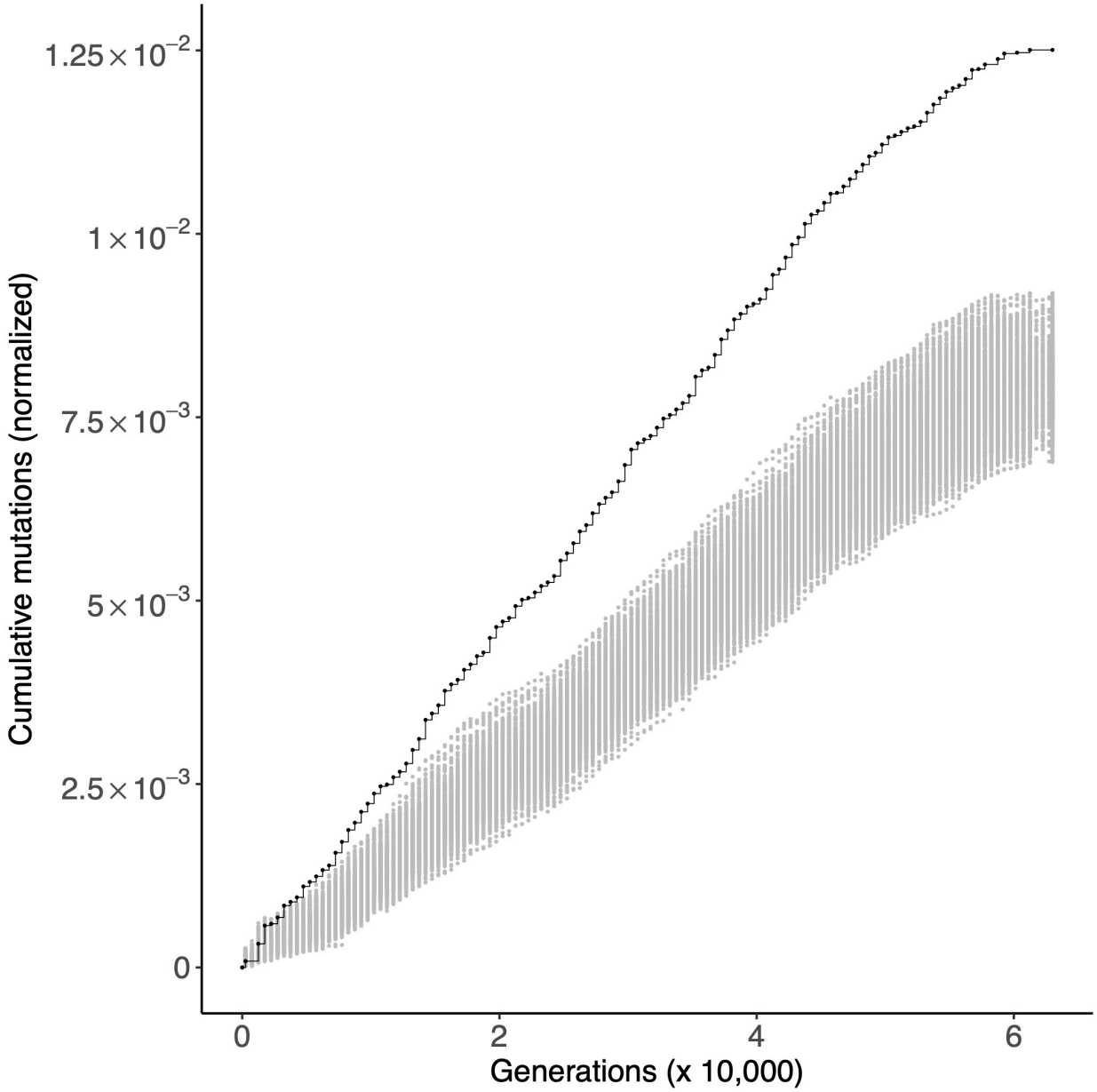

1034
1035

Supplementary Figure S6. Purifying selection on the proteome U-sector. Each panel shows the cumulative number of mutations in the A-sector (black), S-sector (red), O-sector (blue), U-sector (green), R-sector (yellow), and C-sector (orange) in the 12 LTEE populations. For comparison, random sets of 92 genes (i.e. the smallest proteome sector cardinality) were sampled 1,000 times, and the cumulative number of mutations in those random gene sets, normalized by gene length, were calculated. The middle 95% of this null distribution is shown in gray. The top six panels are the nonmutator populations and the bottom six panels are the hypermutator populations.

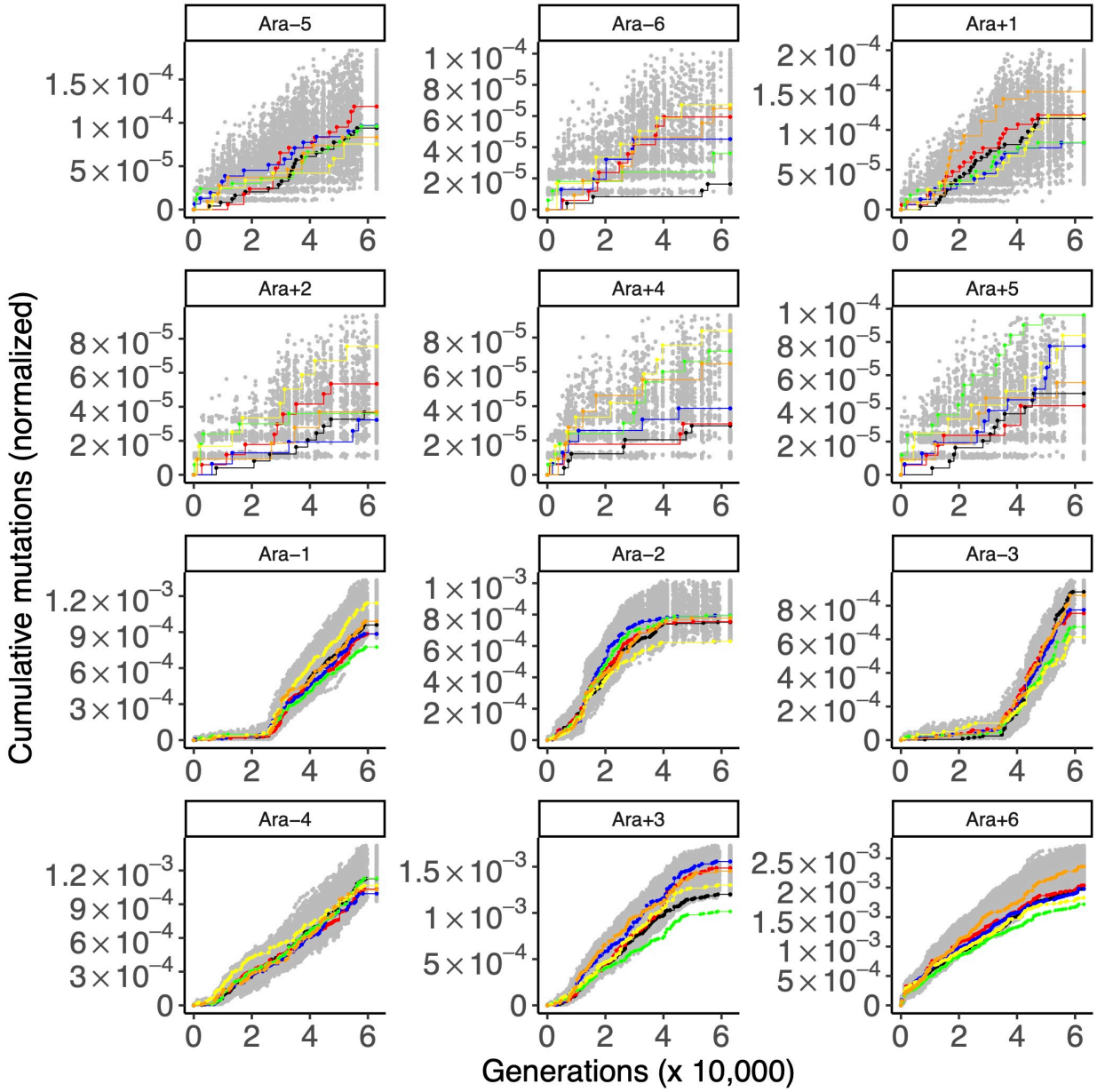

1047 **Supplementary Figure S7. Purifying selection on the proteome U-sector and R-sector.** Each
1048 panel shows the cumulative number of mutations in the A-sector (black), S-sector (red), O-sector
1049 (blue), U-sector (green), R-sector (yellow), and C-sector (orange) in all 12 LTEE populations.
1050 For comparison, random sets of 92 genes (i.e. the smallest proteome sector cardinality) were
1051 sampled 1,000 times, and the cumulative number of mutations in those random gene sets,
1052 normalized by gene length, were calculated. The middle 95% of this null distribution is shown in
1053 gray.
1054

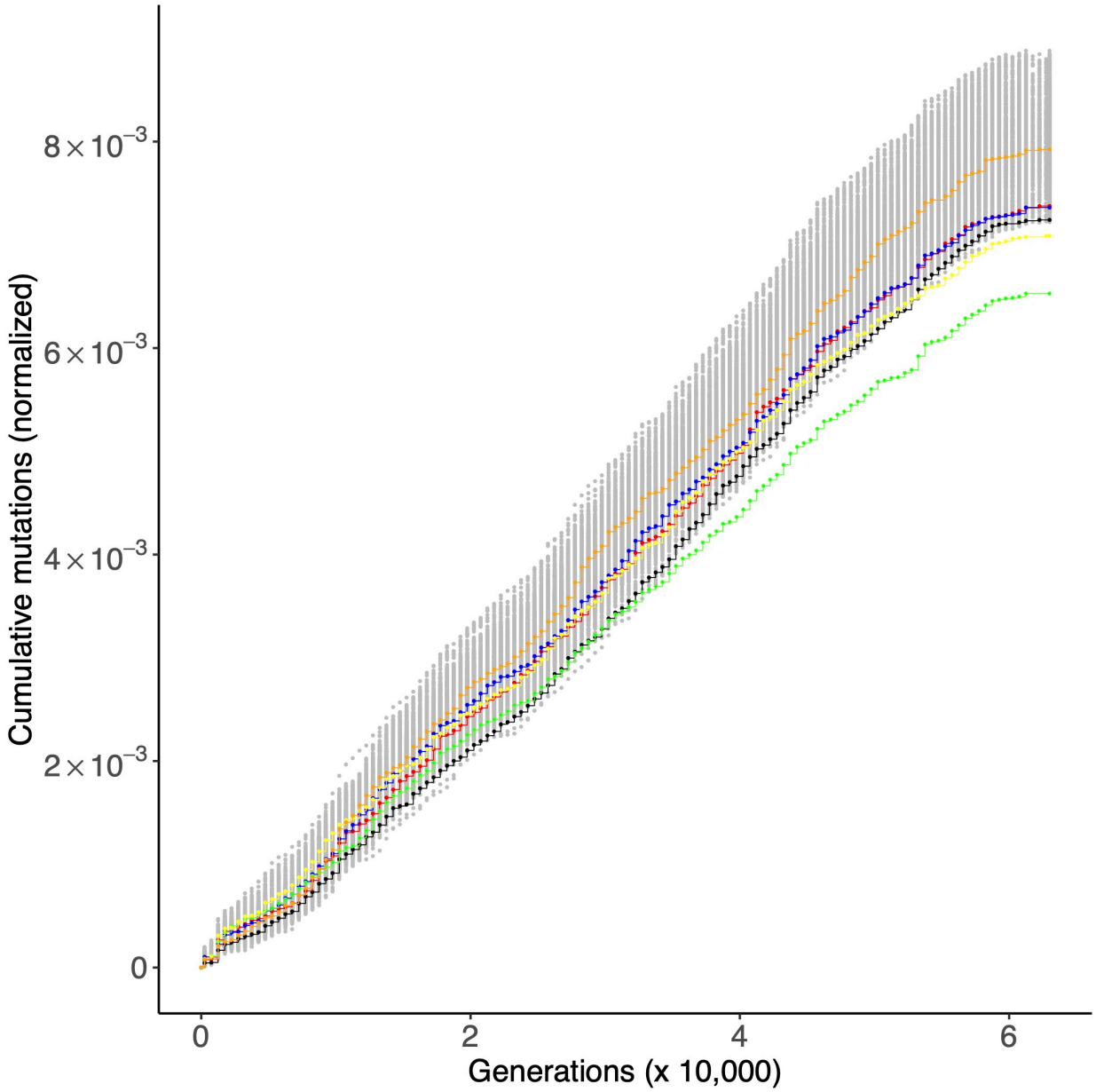

1055

Supplementary Figure S8. No evidence of selection on *E. coli* eigengenes. Each panel shows the cumulative number of mutations in eigengene 1 (red), eigengene 2 (orange), eigengene 3 (yellow), eigengene 4 (green), eigengene 5 (cyan), eigengene 6 (blue), eigengene 7 (violet), eigengene 8 (pink), and eigengene 9 (black) in the 12 LTEE populations. For comparison, random sets of 15 genes (i.e. the smallest eigengene cardinality) were sampled 1,000 times, and the cumulative number of mutations in those random gene sets, normalized by gene length, were calculated. The middle 95% of this null distribution is shown in gray. The top six panels are the nonmutator populations and the bottom six panels are the hypermutator populations.

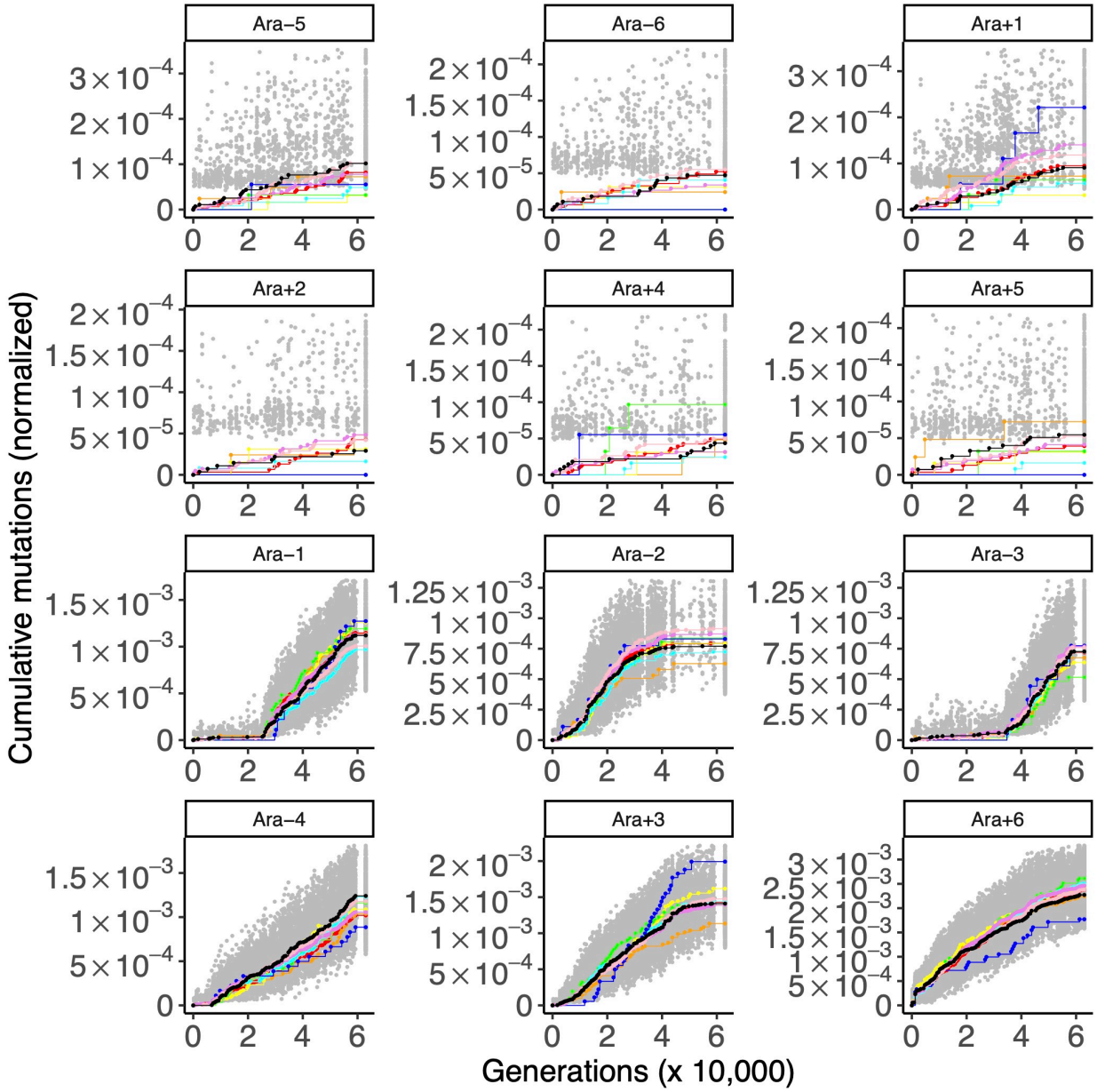

1069 **Supplementary Figure S9. No evidence of selection on *E. coli* eigengenes.** Each panel shows
1070 the cumulative number of mutations in eigengene 1 (red), eigengene 2 (orange), eigengene 3
1071 (yellow), eigengene 4 (green), eigengene 5 (cyan), eigengene 6 (blue), eigengene 7 (violet),
1072 eigengene 8 (pink), and eigengene 9 (black) in the 12 LTEE populations. For comparison,
1073 random sets of 15 genes (i.e. the smallest eigengene cardinality) were sampled 1,000 times, and
1074 the cumulative number of mutations in those random gene sets, normalized by gene length, were
1075 calculated.
1076

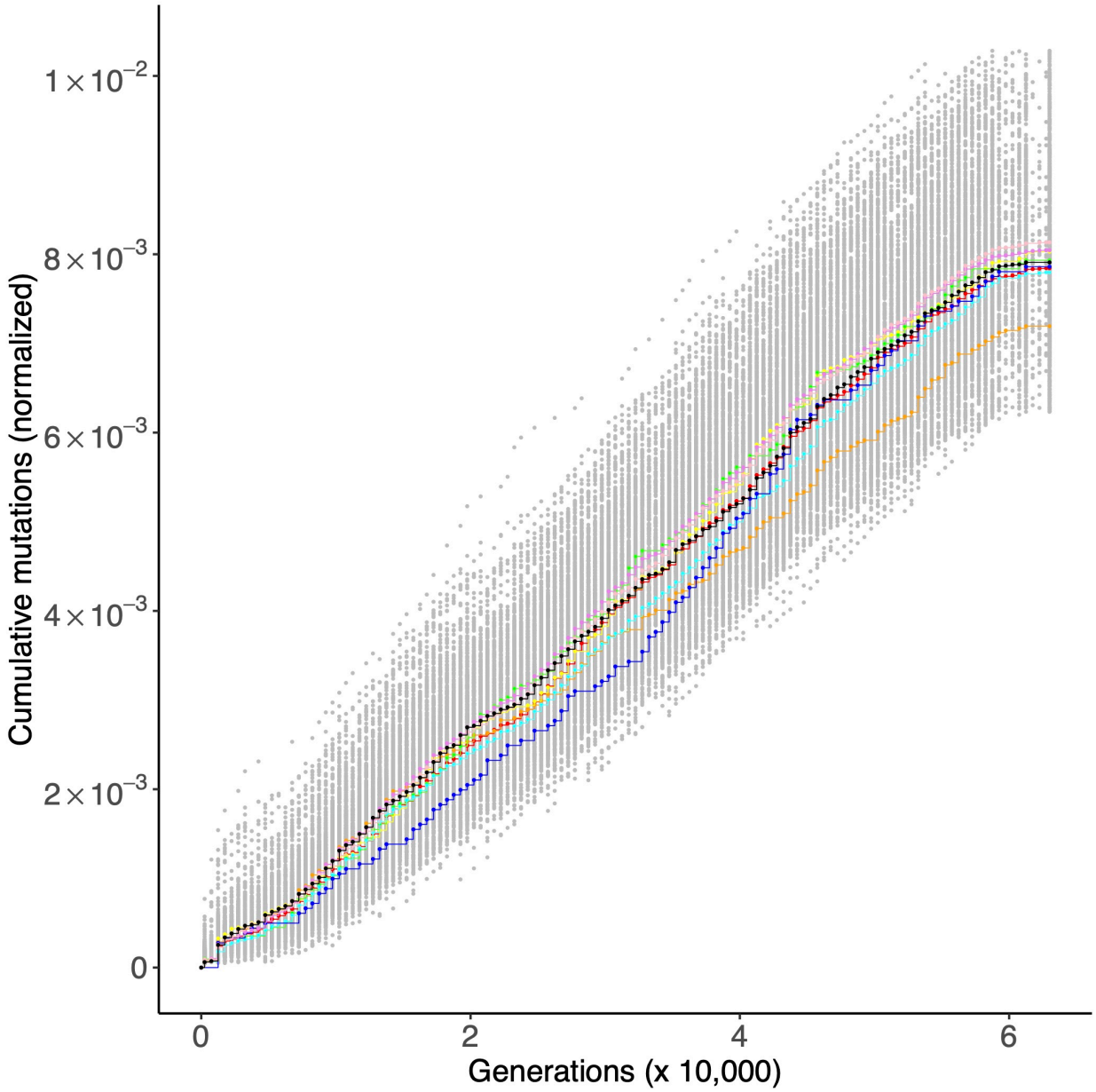

1077

1078 **Supplementary Figure S10. I-modulon regulators evolve under strong positive selection,**
1079 **while genes regulated within I-modulon evolve under purifying selection.** Each panel shows
1080 the cumulative number of mutations in 70 I-modulon regulators (black) and in 1,394 genes
1081 regulated by I-modulon regulators (red) in the 12 LTEE populations. For comparison to the I-
1082 modulon regulators, random sets of 70 genes were sampled 1,000 times, and the cumulative
1083 number of mutations in those random gene sets, normalized by gene length, were calculated. The
1084 middle 95% of this null distribution is shown in gray. A similar procedure was used with random
1085 sets of 1,394 genes to make a comparable distribution in pink to compare to the genes regulated
1086 by I-modulon regulators.
1087

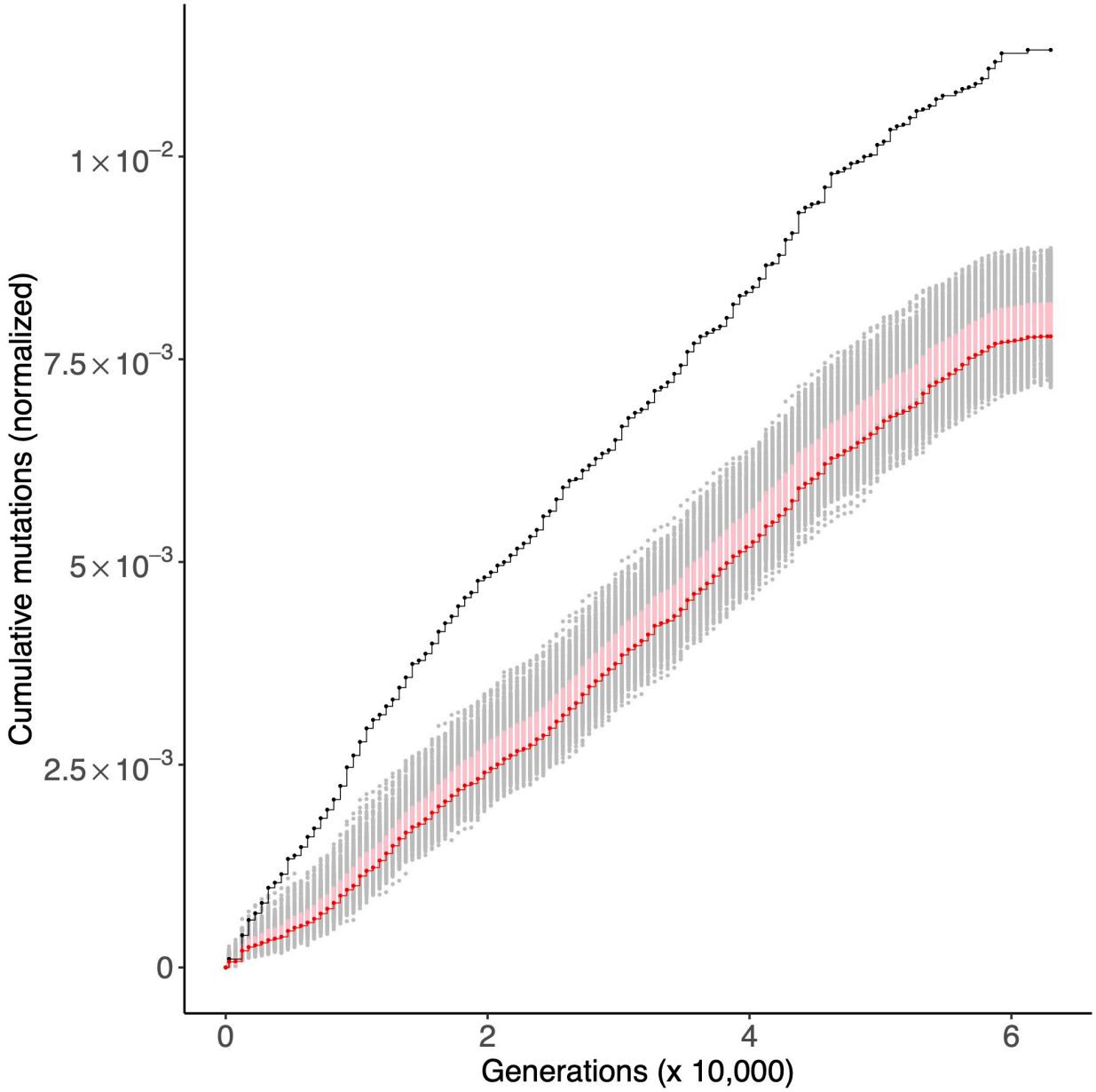

1088

1089 **Supplementary Figure S11. Regulatory genes are under positive selection in hypermutator**
1090 ***Pseudomonas aeruginosa* populations evolving under subinhibitory concentrations of**
1091 **colistin.** Each panel shows the cumulative number of mutations in 424 annotated regulatory
1092 genes (black), in two replicate populations of hypermutator *P. aeruginosa*. For comparison,
1093 random sets of 424 genes were sampled 1,000 times, and the cumulative number of mutations in
1094 those random gene sets, normalized by gene length, were calculated. The middle 95% of this null
1095 distribution is shown in gray.
1096

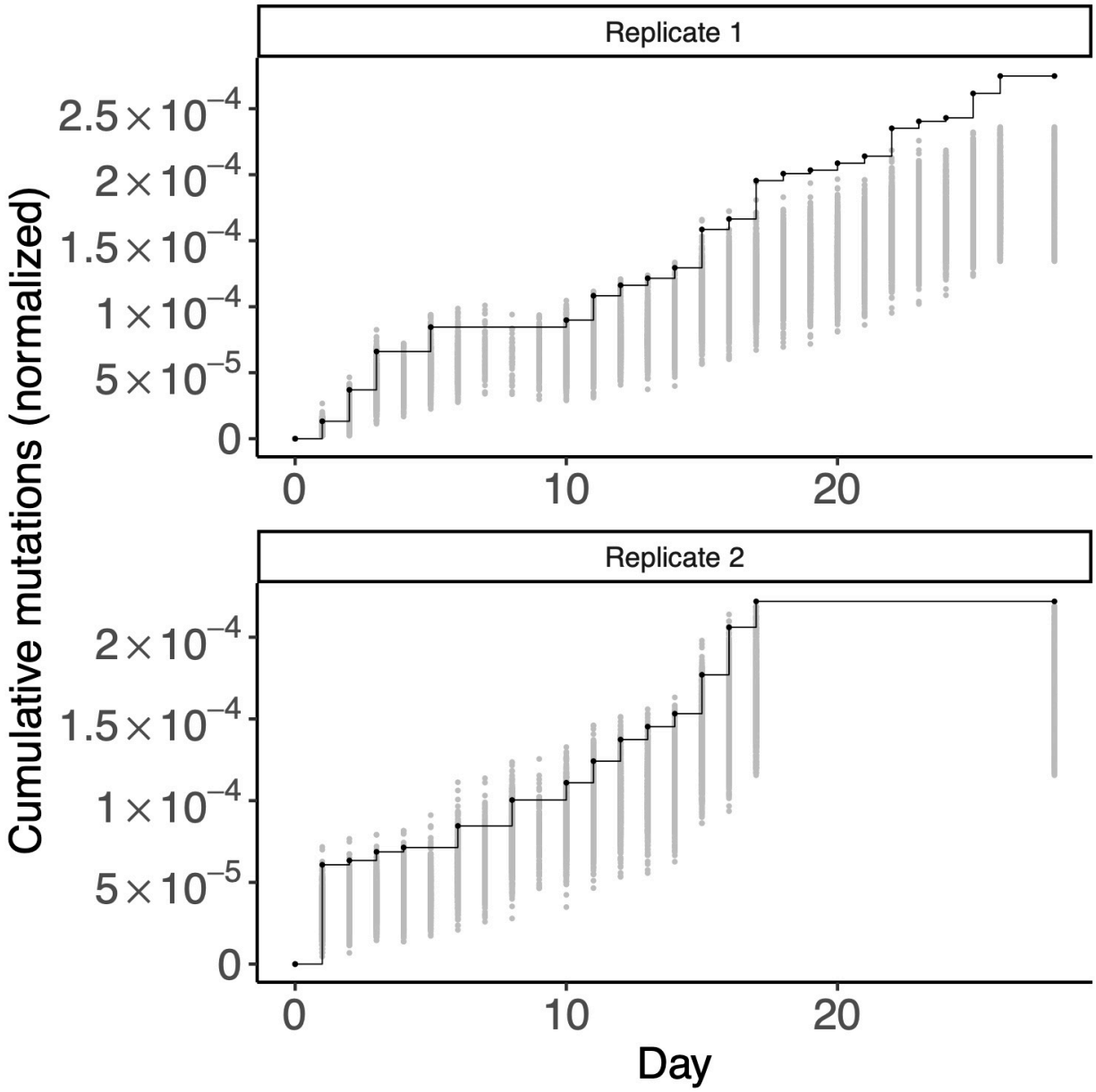

1097
1098